Redox Biology 41 (2021) 101904

Contents lists available at ScienceDirect

Redox Biology

journal homepage: www.elsevier.com/locate/redox

bFGF alleviates diabetes-associated endothelial impairment by downregulating inflammation via S-nitrosylation pathway

Gen Chen [a,b,1], Ning An [c,1], Weijian Ye [d], Shuai Huang [e], Yunjie Chen [a], Zhicheng Hu [a], Enzhao Shen [a], Junjie Zhu [a], Wenjie Gong [a], Gaozan Tong [a], Yu Zhu [a], Lexuan Fang [f], Chunyuan Cai [g], Xiaokun Li [a], Kwonseop Kim [b,*], Litai Jin [a,*], Jian Xiao [a,*], Weitao Cong [a,*]

[a] School of Pharmaceutical Science, Wenzhou Medical University, Wenzhou, 325000, PR China
[b] College of Pharmacy, Chonnam National University, Gwangju, 500-757, South Korea
[c] Department of Pharmacy, Ningbo Medical Center Lihuili Hospital, Ningbo, 315041, PR China
[d] Department of Pharmacy, The Second Affiliated Hospital and Yuying Children's Hospital of Wenzhou Medical University, Wenzhou, 325027, PR China
[e] Zhejiang Provincial Key Laboratory of Interventional Pulmonology, The First Affiliated Hospital of Wenzhou Medical University, Wenzhou, 325000, PR China
[f] College of Pharmaceutical Science, Zhejiang University of Technology, Hangzhou, China
[g] The Third Affiliated Hospital of Wenzhou Medical University, Wenzhou, 325000, PR China

ARTICLE INFO

Keywords:
Diabetes mellitus
bFGF
S-nitrosylation
Inflammation
NFκB
Angiogenesis

ABSTRACT

Protein S-nitrosylation is a reversible protein modification implicated in both physiological and pathophysiological regulation of protein function. However, the relationship between dysregulated S-nitrosylation homeostasis and diabetic vascular complications remains incompletely understood. Here, we demonstrate that basic fibroblast growth factor (bFGF) is a key regulatory link between S-nitrosylation homeostasis and inflammation, and alleviated endothelial dysfunction and angiogenic defects in diabetes. Subjecting human umbilical vein endothelial cells (HUVECs) to hyperglycemia and hyperlipidemia significantly decreased endogenous *S*-nitrosylated proteins, including S-nitrosylation of inhibitor kappa B kinase β ($IKK\beta^{C179}$) and transcription factor p65 ($p65^{C38}$), which was alleviated by bFGF co-treatment. Pretreatment with carboxy-PTIO (c-PTIO), a nitric oxide scavenger, abolished bFGF-mediated S-nitrosylation increase and endothelial protection. Meanwhile, nitrosylation-resistant $IKK\beta^{C179S}$ and $p65^{C38S}$ mutants exacerbated endothelial dysfunction in *db/db* mice, and in cultured HUVECs subjected to hyperglycemia and hyperlipidemia. Mechanistically, bFGF-mediated increase of S-nitrosylated IKKβ and p65 was attributed to synergistic effects of increased endothelial nitric oxide synthase (eNOS) and thioredoxin (Trx) activity. Taken together, the endothelial protective effect of bFGF under hyperglycemia and hyperlipidemia can be partially attributed to its role in suppressing inflammation via the S-nitrosylation pathway.

1. Introduction

Metabolic syndrome and type 2 diabetes mellitus (T2DM) are associated with insulin resistance, hyperglycemia, and hyperlipidemia, which contribute to the chronic inflammation implicated in diabetic vascular complications [1]. Diabetic vascular complications are major causes of shortened life expectancy and high mortality among persons with diabetes [2].

Protein S-nitrosylation is a highly-conserved, nitric oxide (NO)-dependent post-translational cysteine modification, which regulates protein structure and function in bacteria, plants, and mammals [3,4]. More than 3000 S-nitrosocysteine sites have been identified by high-throughput proteomic analyses of *in vitro* and *in vivo* S-nitrosylated proteins (PSNOs) [5]. In individual cells, the steady-state concentration of PSNOs reflects the equilibrium between protein and low-molecular-weight SNOs, which are regulated by rates of S-nitrosylation and denitrosylation. S-nitrosylation is a function of NO synthesis, and is catalyzed by nitric oxide synthases (NOSs) and nitrosylase enzymes, which directly introduce NO into proteins [6]. Denitrosylation is catalyzed by denitrosylases, including the enzymes

* Corresponding authors.
E-mail addresses: koskim@jnu.ac.kr (K. Kim), jin_litai@126.com (L. Jin), xfxj2000@126.com (J. Xiao), cwt97126@126.com (W. Cong).
[1] These authors contributed equally.

https://doi.org/10.1016/j.redox.2021.101904
Received 7 December 2020; Received in revised form 26 January 2021; Accepted 15 February 2021
Available online 20 February 2021
2213-2317/© 2021 The Author(s). Published by Elsevier B.V. This is an open access article under the CC BY-NC-ND license (http://creativecommons.org/licenses/by-nc-nd/4.0/).

S-nitrosoglutathione reductase (GSNOR) [7] and Trx [8,9].

Accumulating evidence suggest that physiological S-nitrosylation contributes to cellular homeostasis, while dysregulation of S-nitrosylation can result in severe pathological consequences [10]. For example, S-nitrosylation of mitochondrial Complex I positively regulates mitochondrial function at the reperfusion phase of myocardial infarction [11]. S-nitrosylation of inositol-requiring enzyme 1 (IRE1) contributes to impaired ER homeostasis in mouse models of obesity [12]. Similarly, S-nitrosylation of endothelial cell proteins also occurs under various physiological and pathophysiological conditions, and plays an important role in regulation of endothelial function [13]. For example, the pro-inflammatory cytokine tumor necrosis factor-alpha (TNF-α) and oxidized LDL (oxLDL) both decrease endothelial protein *S*-nitrosylation [14]. Also, high glucose-induced superoxide production in endothelial cells induces degradation of protein *S*-nitrosothiols in a dose- and time-dependent manner [16]. Contrastingly, exposure to shear stress globally increases endothelial cell protein *S*-nitrosylation [15].

Basic fibroblast growth factor (bFGF), a single-chain polypeptide comprised of 146 amino acids, have been investigated in the fields of wound healing [17], bone regeneration [18], acute ischemia [19], and myocardial infarction [20], both experimentally and clinically. However, the effects of bFGF on endothelial S-nitrosylation homeostasis in diabetes have not yet been evaluated. In the present study, we sought to examine the link between dysregulation of S-nitrosylation and endothelial dysfunction in T2DM to determine whether bFGF could alleviate endothelial dysfunction in this context by mediating cellular S-nitrosylation homeostasis and, if so, to delineate the responsible mechanisms of action.

2. Materials and Methods

2.1. Animal procedures

Diabetic db/db mice and their control littermates, db/m, were obtained from Jackson Laboratories (Strain: BKS. Cg-Dock 7^{m} +/+ $Lepr^{db}$/J). The mice were housed in an environmentally controlled room for 4–6 days to adapt to the environment before experimentation. After withholding food for 12 h, blood samples were obtained from the tail veins. ALZET® Osmotic Pumps (Model 2004) containing PBS (Gibco BRL, 10010), bFGF (30 μg/kg/day, Thermo Fisher Scientific, CTP0263) or GSNO (10 mg/kg/day, Sigma-Aldrich, N4148) [7] were implanted intraperitoneally and were calibrated to release the drug for 28 days. After a 4-week course of treatment, aortic ring assays were performed. Blood glucose level at different time points were measured by glucose analyzer (Lifescan Surestep).

Male C57BL/6 mice (6–8 weeks, 18–23g), were purchased from the Model Animal Research Center of Nanjing University (Nanjing, China). All animal were kept in a standard laboratory condition of temperature 21 ± 2 °C, relative humidity 50 ± 15%, 12 h light-darkness cycles, with water and food available ad libitum. All animal experiments and methods performed in this study followed ethical guidelines for animal studies and were approved by the Institutional Animal Care and Use Committee of Wenzhou Medical University, China.

2.2. Cell culture and treatments

HUVECs were purchased from Lonza and cultured in endothelial cell growth medium-2 (EGM-2; BulletKit, Lonza, CC-3156 and CC-4176) until the start of the experiment. Subconfluent cells (5–7 passages) were used in the experiments. Before starting the experimental procedures, the medium was removed and replaced with phenol red-free low-glucose D-MEM (Gibco BRL, 11054020) supplemented with 1% calf serum (Gibco BRL, 16010159) for 12 h, then HUVECs were placed in EGM-2 consisting of either NG (5.5 mM) or HG + PA (33 mM HG +10 nM PA) in the presence or absence of bFGF (20 ng/mL, Thermo Fisher Scientific, PHG0369) [21] for 72 h; MAN (33 mM: 5.5 mM of glucose + 27.5 mM of D-mannitol) was used as the osmotic control for HG. Media were changed every 24 h.

When analyzing the alteration of eNOS and iNOS, HUVECs were cultured in HG medium for 2 days, 3 days, 4 days and 5 days, respectively. For signaling pathway analysis, each pathway antagonist: compound C [22] (10 μM; Selleck Chemicals, S7306), LY294002 [23] (20 μM; Sigma-Aldrich, L9908), carboxy-PTIO [24] (100 μM; Sigma-Aldrich, 217386) or BJG398 [25] (10 nM; Selleck Chemicals, S2183) were given as pretreatment for 2 h every day before bFGF administration. In some experiments, HUVECs were exposed to HG + PA in combination with the NO donor GSNO [26] (100 μM) for 72 h.

2.3. Immunoblotting analysis

Proteins were extracted from cells and subjected to SDS–polyacrylamide gel electrophoresis, as previously described [27]. Primary antibodies included: p-$eNOS^{S1177}$ (CST, 9571), eNOS (CST, 32027), iNOS (Abcam, ab3523), p-AKT^{S473} (CST, 4060), AKT (CST, 4691), p-$GSK3\beta^{S9}$ (CST, 9323), GSK3β (CST, 9315), p-$AMPK\alpha^{T172}$ (CST, 2535), AMPK (CST, 2603), p65 (CST, 8242), IKKβ (Abcam, ab178870), Biotin (Abcam, ab1227), Trx (CST, 2429), TrxR (CST, 6925), Txnip (CST, 14715), GSNOR (Abcam, ab177932). The expression of β-Actin (Abcam, ab8226) was used as a loading control.

2.4. RNA isolation and quantitative real-time-PCR (qRT-PCR)

Total RNA was extracted from HUVECs by using TRIzol Reagent (Invitrogen, 15596018) according to the manufacturer's instructions. Next, total RNA (2 μg) was reverse transcribed into cDNA by using GoScript Reverse Transcription Kit (Promega, A5001). Quantitative RT-PCR analysis was performed using PowerUp SYBR Green Master Mix (Thermo Fisher Scientific, A25918). Data were analyzed and normalized with *β-Actin*. Gene-specific primer sequences used for qRT-PCR are listed in Supplementary Information Table S3.

2.5. Construction of adenovirus

Recombinant adenovirus vectors were constructed, propagated and tittered as previously described [28]. We made replication-defective human adenovirus type 5 (devoid of E1) harboring human $p65^{WT}$ (*Ad-Cdh5-p65^{WT}*), $p65^{C38S}$ (*Ad-Cdh5-p65^{C38S}*); $IKK\beta^{WT}$ (*Ad-Cdh5-IKKβ^{WT}*), $IKK\beta^{C179S}$ (*Ad-Cdh5-IKKβ^{C179S}*) and human Txnip (*Ad-Txnip*). The Cdh5 promoter ensures restriction of transgene expression in endothelium which was originally described [29], and an in-house-generated *Ad-LacZ* was used as a control. For adenovirus-mediated gene transfer, these constructed adenovirus vectors were transfected into HUVECs at a MOI of 100 × PFU/cell for 24 h.

2.6. Construction of shRNA adenoviral expression vectors

The pSilencer 2.1-U6 expression vector was purchased from Ambion (Ambion, AM5762). The RNU6-1 RNA polymerase III promoter and the polylinker region were subcloned into the adenoviral shuttle vector pDC311 (Microbix, PD-01-25). The human *eNOS-shRNA* targeting sequence was 5′-GTGGCCAACGCCGTGAAGATC-3′. The human *iNOS-shRNA* targeting sequence was 5′-GGTAACAAAGGAGATAGAAAC-3′. The human *Trx-shRNA* targeting sequence was 5′-GCAGGTGATAAACTTGTAGTA-3′. For Scrambled shRNA, an in-house-generated shRNA adenovirus that encodes a scrambled sequence was used as control. For adenovirus-mediated gene knockdown, these constructed adenovirus vectors were transfected into HUVECs at a MOI of 20 × PFU/cell for 24 h.

2.7. Lentiviral vector construction, virus production and titration

To construct a lentiviral vector overexpressing the human $p65^{WT}$

(*LV-EGFP-Neo-p65^{WT}-3Flag*), p65^{C38S} (*LV-EGFP-Neo-p65^{C38S}-3Flag*); IKKβ^{WT} (*LV-EGFP-Puro-IKKβ^{WT}-3Flag*), IKKβ^{C179S} (*LV-EGFP-Puro-IKKβ^{C179S}-3Flag*), the PCR product was digested with XbaI and Xho I, and then ligated into the lentiviral backbone plasmid *pLenti-EF1a-EGFP-P2A-Neo-CMV-3Flag* and *pLenti-EF1a-EGFP-P2A-Puro-CMV-3Flag* respectively by T4 DNA ligase (TaKaRa, 2011B). An in-house-generated *LV-LacZ* was used as a control. For lentivirus-mediated gene transfer, these constructed lentiviral vectors were transfected into HUVECs at a MOI of 100 × PFU/cell for 48 h. After 48 h, a stable p65^{WT}, p65^{C38S}, IKKβ^{WT}, IKKβ^{C179S} overexpression cells was established and selected with puromycin (BD Biosciences, B7587) and G418 (Selleck Chemicals, S3028), respectively.

2.8. Measurement of trx activity

Trx activity was measured using the insulin disulfide reduction assay as described elsewhere [30]. Briefly, Total cellular protein was extracted with lysis buffer. Cellular protein (40 μg) extracts were incubated with activation buffer at 37 °C for 15 min before they were incubated with Trx reductase (Sigma-Aldrich, T7915) in the reaction buffer at 37 °C for 30 min. Distilled water was loaded as a control. Finally, the reaction was terminated by stopping buffer. The absorbance was assessed using a multifunctional microplate reader (SpectraMax M5; Molecular Devices) at a wavelength of 412 nm. Trx activity was expressed as nicotinamide adenine dinucleotide phosphate oxidized per minute per milligram of protein (μM/min/mg).

2.9. Measurement of GSNOR enzymatic activity

HUVECs were prepared on ice in a solution. The GSNOR activity was measured by GSNO-dependent NADH (reduced form of NAD^+) consumption [31]. Briefly, cell lysate (0.3 mg/mL) was incubated with 75 μM NADH in reaction buffer containing 0 or 100 μM GSNO at room temperature, and NADH fluorescence (absorption at 340 nm and emission at 455 nm) was measured over time to determine the initial rate of GSNO-dependent NADH consumption.

2.10. Biotin-switch assay

S-nitrosylated proteins were detected by using the biotin-switch assay [32] with some modifications. In brief, lysates (50 mL) were incubated in HENS buffer and 20 mM methyl methanethiosulfonate (MMTS) at 50 °C for 20 min. Proteins were precipitated with cold acetone, washed twice, resuspended in HENS, and mixed with 0.2 mM biotin-HPDP (BD Biosciences, A8008) and 2.5 mM ascorbate at ambient temperature for 1 h. Finally, biotinylated proteins were purified by using streptavidin-agarose beads (Sigma-Aldrich, GE90100484), separated by SDS-PAGE, and detected by immunoblotting.

2.11. Fluorescent detection of S-Nitrosylation and immunofluorescence

Biotin-switch assay was performed on fixed and permeabilized HUVECs by first blocking free thiols using HENS buffer containing 20 mM MMTS at 50 °C for 20 min. Nitrosothiols were labeled in HENS buffer (1% SDS), 0.4 mM biotin-HPDP and 1 mM ascorbic acid at ambient temperature for 1 h. Biotinylated proteins were visualized by using avidin conjugated with Alexa 568 (Thermo Fisher Scientific, S11226). Finally, cells were analyzed using a confocal laser scanning microscope (Leica TCS SP8, Wetzlar, Germany).

2.12. Electrophoretic mobility shift assay

DNA binding of NFκB was measured by performing electrophoretic mobility shift assay (EMSA) as previously described [33]. Binding reactions were resolved on a 4% nondenaturing polyacrylamide gel at 22 mA for 30 min at 4 °C in 0.5 × TBE. Samples were then electrotransferred onto positively charged nylon membrane and subjected to antibody reaction. Finally, chemiluminescent detection following ChemiDoc MP device (Bio-Rad, Hercules, CA, USA) and densitometry was conducted with ImageQuant 5.2 software (Molecular Dynamics, Sunnyvale, CA).

2.13. Luciferase assay

For luciferase reporter assays, firefly luciferase constructs driven by NFκB binding sequences and Renilla luciferase pRL-TK (Int-) plasmid were used (Promega, E2271). Lysates were analyzed with the Dual-Luciferase Reporter Assay System (Promega, E1910). Firefly luciferase and Renilla luciferase were detected on a Veritas Microplate Luminometer (Promega, Madison, WI, USA).

2.14. In vitro angiogenesis (tube formation) assay

The *in vitro* angiogenic activity of HUVECs was determined by Matrigel tube formation assay. Capillary-like tube formation was observed with a computer-assisted microscope (EVOS, Thermo Fisher Scientific, MA, United States). The tube length in duplicate wells was counted and averaged using ImageJ software (National Institutes of Health, Bethesda, Maryland, USA).

2.15. Aortic ring assay

To establish a direct action of bFGF on vascular, thoracic aortae from db/db and db/m mice after four-week treatment or C57BL/6 mice were surgically isolated, cleaned and dissected into 0.5 mm rings, then rings were embedded in fibrin [34,35].

For lentivirus-mediated gene transfer, these constructed lentiviral vector were transfected aortic rings from db/db and db/m mice respectively at 30–50 rings per well of a 24-well plate by adding 0.5 mL of Opti-MEM (Gibco BRL, 51985–026) and 1 × 10^8 vector genome copies to each well for 48 h as described previously [14]. Before the regression phase, rings were fixed for immunofluorescence staining of CD31 (Abcam, ab24590). Pictures were taken on day 12, and the total number of branches was counted using ImageJ (National Institutes of Health, Bethesda, Maryland, USA).

2.16. Wound healing scratch assay

Cell migration was determined using the wound healing scratch assay as previously described [36]. Cells were seeded on 6-well plates and grown overnight, until forming a confluent monolayer and a scratch was made using a 200 μL pipette tip. Images of the wounded cell monolayers were taken using a microscope (EVOS, Thermo Fisher Scientific, MA, United States) at 0 and 36 h after wounding and controlled by ImageJ software (National Institutes of Health, Bethesda, Maryland, USA). All experiments were performed in the presence of Mitomycin-C (10 μM, Selleck Chemicals, S8146) [37] to inhibit cell proliferation.

2.17. Wound-healing assay

General anesthesia was performed with 2% inhaled isoflurane and then injected subcutaneously with the analgesic. Two full-thickness wounds were created on the shaved dorsal skin of each of the 8-week-old db/db mice and db/m mice using 8 mm skin biopsy punches, then each wound covered hydrogel scaffolds respectively including PBS, bFGF (30 ng/mL) and GSNO (150 μM) with a diameter of 10 mm, and bandaged with sterile cotton-cloth. In addition, to evaluate rescue effects, adenoviruses expressing endothelium-specific p65^{WT} (*Ad-Cdh5-p65^{WT}*), p65^{C38S} (*Ad-Cdh5-p65^{C38S}*); IKKβ^{WT} (*Ad-Cdh5-IKKβ^{WT}*), IKKβ^{C179S} (*Ad-Cdh5-IKKβ^{C179S}*) and *Ad-LacZ* (control) were injected intradermally into the wound edges in the db/db mice and db/m mice the day after wounding, and the wound closure rate was measured [38].

The wound areas remaining open were calculated as follows: wound areas remaining open (%) = (open area on the indicated day/original wound area) × 100%. Paraffin-embedded tissue sections (5 μm in thickness) were deparaffinized and rehydrated, followed by H&E staining. Reepithelization ratios (leading edge ratios) were measured and calculated by [(a + b)/c] × 100% (shown in Supplementary Fig. 5d, where a and b are the length of the axes for the leading edges, and c indicates the axis of initial wound lengths) [39]. Blood fasting glucose levels were measured during the experiment (Supplementary Information Table S2).

2.18. Immunofluorescence for CD31 staining

Capillary density in wound skin tissues were determined as reported [40]. Briefly, Paraffin-embedded tissue sections (5 μm in thickness) were deparaffinized and rehydrated, then fixed with 4% (w/v) paraformaldehyde for 20 min and permeabilized with 0.5% (v/v) Triton X-100 for 20 min at 37 °C. After wash, the cells were blocked in 2% (v/v) BSA for 2 h and incubated with primary Rabbit antibody against CD31 (Abcam, ab24590) at 4 °C overnight. After incubation and wash, cells were blocked with Alexa fluor 647-conjugated anti-rabbit IgG secondary antibody for 1 h. After washes with PBS, the cell nuclei were stained with DAPI for 15 min. The stained wound skin tissues were imaged with a confocal laser scanning microscope (Leica TCS SP8, Wetzlar, Germany). The total tissue area and the CD31 stained positive area were measured with ImageJ software (National Institutes of Health, Bethesda, Maryland, USA). Data were expressed as percentage of positive staining area per analyzed area.

2.19. Immunoprecipitation

HUVECs were lysed with IGEPAL CA-630 buffer (50 mM Tris-HCl, pH 7.4, [Sigma-Aldrich, T5030], 1% IGEPAL CA-630 [Sigma-Aldrich, I8896], 10 mM EDTA, 150 mM NaCl, 50 mM NaF, 1 μM leupeptin [Sigma-Aldrich, L5793], 0.1 μM aprotinin [Sigma-Aldrich, SRE0050]). After immunoprecipitation, the samples were washed with TBS 5 times. They were then eluted with glycine-HCl (0.1 M, pH 3.5) and the immunoprecipitates were subjected to immunoblotting using specific primary antibodies.

2.20. Isolation of nuclear and cytosolic extracts

The isolation of nuclear and cytosolic extracts was performed in HUVECs with a Nuclear and Cytoplasmic Extraction kit (Thermo Fisher Scientific, 78833) according to the manufacturer's instructions.

2.21. Nitrite/nitrate assay

Nitrite/nitrate production in HUVECs were analyzed by using an Ultra-sensitive assay for nitrite/nitrate assay kit (Sigma-Aldrich, 23479), according to the manufacturer's instructions.

2.22. TUNEL staining

HUVECs were stained with an In Situ Cell Death Detection Kit (Roche, 11684795910) according to the manufacturer's protocol.

2.23. Statistical analysis

The results are presented as mean ± SEM from at least four independent experiments. All analyses were performed with the experimenter blinded to the groups of mice and cultured cells. Statistical comparisons were made with two-tailed Student's *t*-test for two experimental groups or one-way analysis of variance (ANOVA) for multiple groups with SPSS software. For enzymatic activity analyses, Wilcoxon rank-sum test were performed. In the TUNEL^{+} cells analyses, we performed the Mann-Whitney *U* test for the TUNEL-positive cells. If not stated otherwise, asterisks indicate significance: ***p < 0.001, **p < 0.01, *p < 0.05 and n. s. represents no significant. Statistical analyses were done using GraphPad Prism (GraphPad Software).

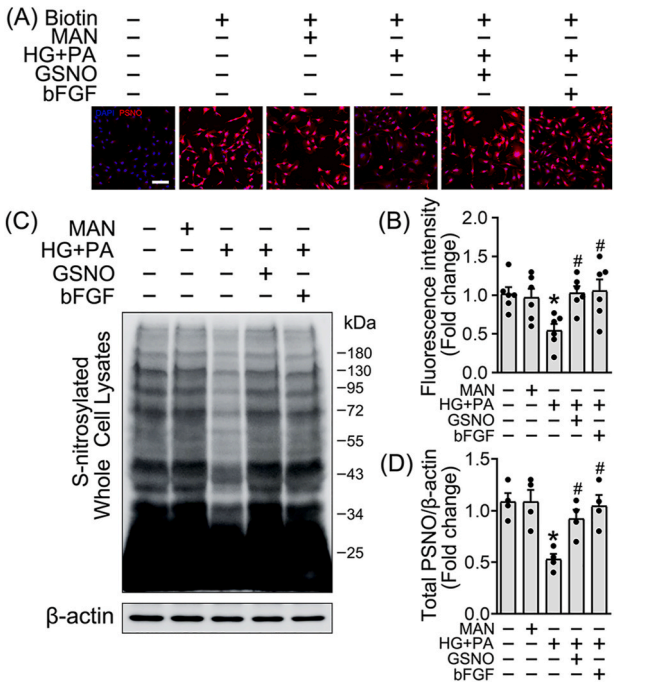

Fig. 1. Effect of bFGF on hyperglycemia and palmitic acid-induced reduction of protein S-nitrosylation. HUVECs were exposed to MAN (33 mM) and HG + PA (33 mM HG + 10 nM PA) in the presence or absence of bFGF (20 ng/mL) or GSNO (100 μM) for 3 days, MAN (33 mM: 5.5 mM of glucose + 27.5 mM of D-mannitol) was served as the osmotic control for the HG. (A) Fixed cells were subjected to a biotin-switch assay. S-nitrosylation was visualized using Alexa-568-conjugated avidin (red) and nuclei were stained with DAPI (blue). Nonspecific staining was determined in control cells incubated with Alexa-568 avidin. Scale bars = 115 μm. (B) The quantitative analysis of fluorescent intensity in at least 6 separate fields, values displayed are means ± SEM of 6 independent experiments. One-way ANOVA Bonferroni's test was used, *p < 0.05 vs. MAN; #p < 0.05 vs. HG + PA. (C) Whole-cell lysates were subjected to the biotin switch assay as described in "Materials and Methods". (D) The quantitative analysis of SNO protein immunoblots, values displayed are means ± SEM of 4 independent experiments. Two-tailed Student's *t*-test was used, *p < 0.05 vs. MAN; #p < 0.05 vs. HG + PA. (For interpretation of the references to colour in this figure legend, the reader is referred to the Web version of this article.)

3. Results

3.1. Effect of bFGF on hyperglycemic and hyperlipidemic impairment of S-nitrosylation

We examined the impact of hyperglycemia and hyperlipidemia (palmitic acid, PA) combined treatment (HG + PA) on S-nitrosylation in HUVECs over 5 days of exposure to HG + PA. 2–3 days of HG + PA treatment decreased protein S-nitrosylation, especially on day 3, but subsequently reversed on days 4–5 (Supplementary Fig. 1A and B). Interestingly, HG + PA exposure for these discrete time points biphasically affected different NOS isoforms. At 2–3 days, activity of endothelial nitric oxide synthase (eNOS) was significantly decreased, while at 4–5 days, expression of inducible nitric oxide synthase (iNOS) gradually increased (Supplementary Fig. 1C and D). Consistently, NO production mimicked both aspects of this phenotype (Supplementary Fig. 1E), suggesting that protein S-nitrosylation was mediated by NO, as was reflected by the corresponding biphasic regulation of eNOS/iNOS activity

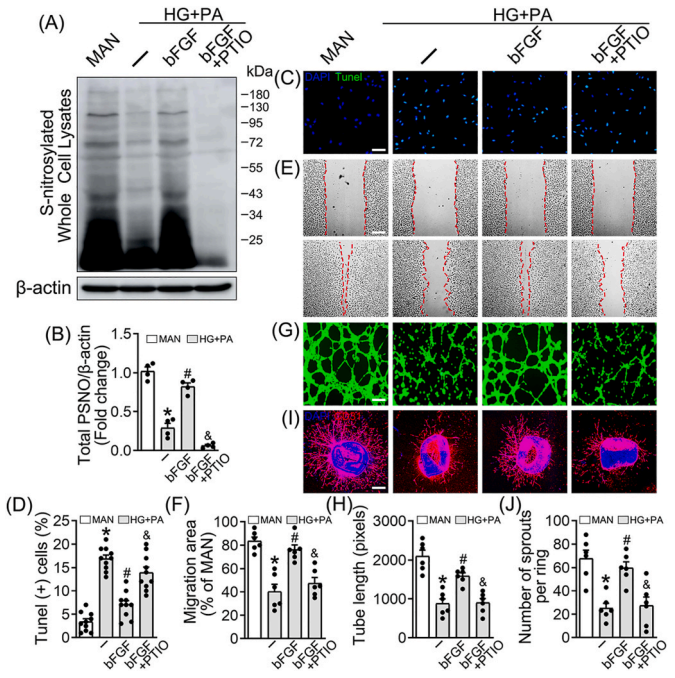

Fig. 2. Decomposition of S-nitrosylation contributes to endothelial dysfunction both *in vitro* and *ex vivo*. HUVECs were cultured either in MAN (5.5 mM) and HG + PA (33 mM HG+10 nM PA) medium in the presence or absence of bFGF (20 ng/mL) or c-PTIO (100 μM) for 72 h. (A) Biotin switch assay of whole-cell lysates. (B) The quantitative analysis of SNO protein immunoblots, the results were normalized to HUVECs exposed to MAN, values displayed are means ± SEM of 4 independent experiments. Two-tailed Student's *t*-test was used. (C) The apoptotic cells were labeled with green, and nuclei were stained with DAPI (blue). Scale bars = 90 μm. (D) The quantitative analysis of $TUNEL^+$ cells in at least 6 separate fields, values displayed are means ± SEM of 10 independent experiments. Non-parametric Mann-Whitney *U* test was used. (E) A scratch wound healing assay was performed in the presence of Mitomycin-C (10 μM). Cell monolayers were imaged at 0 and 36 h after wounding. Red vertical lines indicate the wound area borders. Scale bar = 65 μm. Wound area is analyzed by ImageJ software. (F) Cell migration distances were measured based on the data; values displayed are means ± SEM of 6 independent experiments. One-way ANOVA with Tukey's multiple comparison tests was used. (G) Capillary-like tube formation was assessed by matrigel angiogenesis assay in HUVECs. Scale bar = 85 μm (H) Quantification of the tube length in (G), images of tube morphology were taken in 6 random microscopic fields per sample and values displayed are means ± SEM of 6 independent experiments. Sample means were statistically significant as determined by one-way ANOVA with Bonferroni's correction. (I) Representative images of aortic rings from male C57BL/6 mice cultured in different mediums containing MAN and HG + PA in the presence or absence of bFGF or c-PTIO for 72 h. Scale bars = 350 μm. (J) Quantification of the number of sprouts in (I), one-way ANOVA with Bonferroni's correction was used; values displayed are means ± SEM of 6 independent experiments. Data shown in graphs represent the statistical significance: *p < 0.05 vs. MAN; #p < 0.05 vs. HG + PA; & p < 0.05 vs. exposed to HG + PA in combination with bFGF. (For interpretation of the references to colour in this figure legend, the reader is referred to the Web version of this article.)

or expression.

To determine whether dysregulation of iNOS-induced protein S-nitrosylation altered endothelial function under HG + PA conditions, *iNOS* was knocked down using an adenovirus expressing *iNOS-shRNA*. In HUVECs, *iNOS-shRNA* did not affect S-nitrosylation on days 1–3 of HG + PA treatment, but it eliminated the observed increase of S-nitrosylation on day 5 (Supplementary Fig. 1F and G). These findings were corroborated by whole-cell quantitative nitrite/nitrate production (Supplementary Fig. 1H). The results suggested that iNOS induced endothelial cell protein S-nitrosylation during late-stage exposure to HG + PA, while decreased S-nitrosylation in early-stage exposure was iNOS-independent.

As previous studies have demonstrated that endothelium maintains vascular homeostasis in part by regulating S-nitrosylation homeostasis [13], we hypothesized that bFGF could alleviate HG + PA-induced endothelial dysfunction by correcting aberrations in protein S-nitrosylation. Considering that decreased S-nitrosylation on day 3 of HG + PA exposure was the most important and physiologically relevant aspect of this results, thereby, we sought to determine whether bFGF corrected deficits in S-nitrosylation during early exposure of HUVECs to HG + PA. Firstly, we measured S-nitrosylation of endogenous proteins in the presence or absence of GSNO using biotin-switch assay and immunofluorescence detection of S-nitrosylation in HUVECs (Supplementary Fig. 2). Secondly and consistently, HUVEC protein S-nitrosylation was markedly decreased following 3 days of HG + PA exposure, but was restored by treatment with bFGF or the physiological NO donor S-nitrosoglutathione (GSNO) (Fig. 1C and D). Furthermore, we performed a biotin-switch assay on fixed HUVEC monolayers to visualize S-nitrosylation levels using Alexa-568-labeled avidin [41]. bFGF or GSNO co-treatment markedly increased cytoplasmic and nuclear SNO levels compared with HUVECs exposure to HG + PA (Fig. 1A and B).

To determine whether the effect of bFGF was receptor mediated, HUVECs were treated with the pan-FGFR antagonist BGJ398 (BGJ). BGJ exposure did not affect S-nitrosylation in normal HUVECs, but largely blocked bFGF-mediated restoration of protein S-nitrosylation in HG + PA-treated HUVECs (Supplementary Fig. 3A–D). Together, these data indicated that bFGF elicited receptor-mediated activity to modify protein S-nitrosylation during early exposure of HUVECs to HG + PA.

3.2. *Impaired S-nitrosylation contributed to endothelial dysfunction in vitro and ex vivo*

To determine whether impaired protein S-nitrosylation contributed to endothelial dysfunction in HG + PA conditions, and whether bFGF improved endothelial function by regulating protein S-nitrosylation in this context, HG + PA-treated HUVECs were cultured with bFGF in the presence or absence of the NO scavenger carboxy-PTIO (c-PTIO) for 72 h. Notably, exposure of HUVECs to c-PTIO decreased S-nitrosylated protein levels even in the presence of bFGF (Fig. 2A and B). In parallel, HG + PA impaired cell migration (Fig. 2E and F) and tube-forming capacity (Fig. 2G and H) of HUVECs were improved by bFGF, but counteracted by c-PTIO co-treatment. In addition, bFGF alleviated HG + PA-induced apoptosis in HUVECs, as demonstrated by decreased TUNEL-positive cells (Fig. 2C and D), which was significantly impaired by co-treatment with c-PTIO. These results suggested that bFGF-mediated S-nitrosylation could improve cellular proliferation and migration, and suppress cellular apoptosis.

Next, the *ex vivo* aortic ring sprouting assay was utilized to further assess the endothelial protective effects of bFGF. Aortic rings from male C57BL/6 mice were cultured in HG + PA medium or mannitol (MAN) medium as an osmotic control in the presence or absence of bFGF and/or c-PTIO. In MAN medium, a well-structured microvessel network with clearly defined tubules and regular branching was present. By contrast, aortic rings cultured in HG + PA medium exhibited dramatically impaired sprouting function, which was preserved by bFGF but abolished by c-PTIO co-treatment (Fig. 2I and J). These observations suggested that bFGF mediated regulation of S-nitrosylation under HG + PA conditions alleviated endothelial injury.

3.3. *bFGF-mediated S-nitrosylation of IKKβ and p65 suppressed chronic inflammation*

NFκB is a transcription factor that plays a pivotal role in inflammation, cell survival, and cell proliferation [42], and is maintained in a latent form in the cytoplasm via sequestration by inhibitory κB (IκB) proteins. However, *S*-nitrosylation basally inhibits NFκB activity. Both

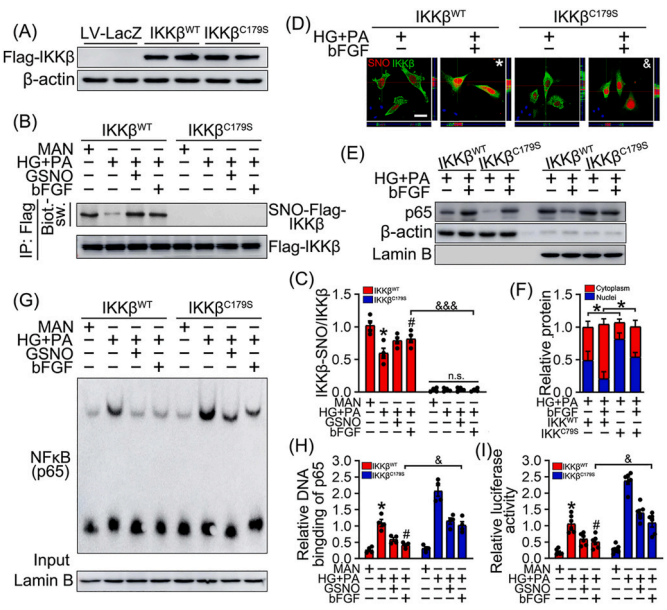

Fig. 3. bFGF mediated SNO-IKKβ contributes to the suppression of chronic inflammation. HUVECs were infected with a lentiviral vector encoding *LacZ* (control), wild-type IKKβ (*LV-IKKβ^{WT}*), or a mutant IKKβ in which Cys-179 was replaced with the non-nitrosylatable residue serine (*LV-IKKβ^{C179S}*). After transfection, overexpression cells were established and selected with puromycin and cultured either in MAN or HG + PA medium in the presence or absence of bFGF and GSNO for 72 h. (A) Representative immunoblotting images of Flag confirmed that the cells were transfected with lentivirus successfully. (B) The mutation of IKKβ^{C179S} abrogated bFGF mediated SNO-IKKβ^{C179}, IKKβ protein loading was detected by anti-Flag antibody. (C) Quantification of S-nitrosylated protein levels (percentage of S-nitrosylated protein to total) in HUVECs, values displayed are means ± SEM of 4 independent experiments. One-way ANOVA with the Student-Newman-Keuls test was used, n. s. = not significant, *p < 0.05 vs. *LV-IKKβ^{WT}*-transfected HUVECs cultured in MAN; #p < 0.05 vs. *LV-IKKβ^{WT}*-transfected HUVECs cultured in HG + PA; &&& p < 0.001 vs. *LV-IKKβ^{WT}*-transfected HUVECs cultured in bFGF. (D) Fixed cells were subjected to a biotin-switch assay. S-nitrosylation was visualized using Alexa-568-conjugated avidin (red) and IKKβ was determined by immunofluorescent staining (green) in HUVECs, the merged puncta (yellow) is the IKKβ closed proximity with S-nitrosated protein or SNO-IKKβ itself, nuclei were stained with DAPI (blue), Scale bars = 200 μm. One-way ANOVA with Bonferroni's correction was used, values displayed are means ± SEM of 3 independent experiments. *p < 0.05 vs. *LV-IKKβ^{WT}*-transfected HUVECs cultured in HG + PA; & p < 0.05 vs. *LV-IKKβ^{WT}*-transfected HUVECs treatment with bFGF. (E) Nuclear and cytosolic extracts made from HUVECs were isolated, and overexpression of non-nitrosylatable IKKβ^{C179S} mutant exposure to bFGF resulted in the nuclear localization of p65. (F) Quantification of p65 localization, values displayed are means ± SEM of 4 independent experiments. One-way ANOVA with the Student-Newman-Keuls test was used, *p < 0.05. (G) EMSA assays were performed as described in "Materials and Methods". Overexpression of non-nitrosylatable IKKβ^{C179S} mutant increases the DNA binding ability of p65. (H) The quantitative analysis of each immunoblots, values displayed are means ± SEM of 4 independent experiments. One-way ANOVA with the Student-Newman-Keuls test was used, *p < 0.05 vs. *LV-IKKβ^{WT}*-transfected HUVECs cultured in MAN; #p < 0.05 vs. *LV-IKKβ^{WT}*-transfected HUVECs cultured in HG + PA; &&& p < 0.001 vs. *LV-IKKβ^{WT}*-transfected HUVECs cultured in bFGF. (I) Equal amounts of cell lysates were tested for luciferase activity as described in "Materials and Methods", values displayed are means ± SEM of 6 independent experiments. One-way ANOVA with the Student-Newman-Keuls test was used, *p < 0.05 vs. *LV-IKKβ^{WT}*-transfected HUVECs cultured in MAN; #p < 0.05 vs. *LV-IKKβ^{WT}*-transfected HUVECs cultured in HG + PA; &&& p < 0.001 vs. *LV-IKKβ^{WT}*-transfected HUVECs cultured in bFGF. (For interpretation of the references to colour in this figure legend, the reader is referred to the Web version of this article.)

subunits of the p50^{C62}-p65^{C38} NFκB heterodimer are targeted for *S*-nitrosylation at a conserved cysteine residue in the Rel DNA binding domain, which disrupts its DNA binding [43]. In addition, the IκB-phosphorylating component of the complex, IKKβ^{C179}, is S-nitrosylated, which suppresses kinase activity and subsequent IκB phosphorylation [44]. Therefore, decreased S-nitrosylation under HG + PA could potentially activate NFκB, and then result to inflammation.

Based on the above prior findings, we sought to determine whether endogenous *S*-nitrosylation of IKKβ or NFκB was altered by HG + PA and subsequently triggered the chronic inflammation. To test this hypothesis, we measured ascorbate-dependent basal S-nitrosylation of endogenous p65 and IKKβ in HUVECs subjected to HG + PA (Supplementary Fig. 4A). HG + PA decreased p65 and IKKβ S-nitrosylation, but largely restored by bFGF or GSNO co-treatment (Supplementary Fig. 4B and C). Meanwhile, bFGF suppressed HG + PA-triggered nuclear translocation of the p65 NFκB subunit (Supplementary Fig. 4D and E) were further confirmed by immunofluorescence (Supplementary Fig. 4F). In addition, NFκB DNA binding and transcriptional activity were evaluated using an electrophoretic mobility shift assay (EMSA) (Supplementary Fig. 4G, H) and a luciferase assay, respectively (Supplementary Fig. 4I). These observations suggested that bFGF increased S-nitrosylation of p65 and IKKβ could alleviate HG + PA-induced inflammation.

To assess the detailed mechanism of bFGF mediated SNO-IKKβ and subsequent endothelial protection, HUVECs were infected with a lentiviral vector encoding *LacZ* (control), wild-type IKKβ (*LV-IKKβ^{WT}*), or a mutant IKKβ in which Cys-179 was replaced with the non-nitrosylatable residue serine (*LV-IKKβ^{C179S}*), and the expression was confirmed by immunoblotting (Fig. 3A). Consistent with a prior report [44], mutation of IKKβ^{C179S} abrogated bFGF-mediated SNO-IKKβ^{C179} (Fig. 3B and C). Additionally, with the immunofluorescence staining of protein S-nitrosylation and IKKβ, we found that bFGF induced the colocalization of S-nitrosated protein (red) with IKKβ (green), which was prevented by the mutant, suggesting that SNO-IKKβ^{C179S} attenuated bFGF-mediated protein S-nitrosylation including SNO-IKKβ at these residues (Fig. 3D). Besides, this mutation also led to the phosphorylation and degradation of the IκB protein, and subsequently triggered nuclear localization of the p65 NFκB subunit (Fig. 3E and F) and initiation of NFκB-dependent gene transcription, as assessed by EMSA (Fig. 3G and H) and luciferase assay (Fig. 3I). By contrast, these changes were not observed in MAN conditions (Fig. 3B–I). These observations demonstrated that the IKKβ^{C179S} mutation abrogated bFGF restrained NFκB signaling, indicating that bFGF suppress NFκB by regulating S-nitrosylation of IKKβ.

In parallel, to evaluate the importance of SNO-p65 in bFGF restrained NFκB, HUVECs were infected with a lentiviral vector encoding *LacZ* (control), wild-type p65 (*LV-p65^{WT}*), or mutant p65, in which Cys-38 was replaced with the non-nitrosylatable residue serine (*LV-p65^{C38S}*), and the expression was confirmed by immunoblotting (Fig. 4A). Similarly, the p65^{C38S} mutation also abrogated bFGF restrained NFκB (Fig. 4B and C). Meanwhile, bFGF-induced suppression of NFκB transcriptional activity was partially abolished in *LV-p65^{C38S}*-infected HUVECs (Fig. 4G–I), without affecting the nuclear localization of p65 (Fig. 4D and E). Additionally, bFGF mediated protein S-nitrosylation (red) including SNO-p65 (partially yellow puncta) were also largely attenuated in non-nitrosylatable p65^{C38S} mutant HUVECs (Fig. 4F). Therefore, we ascertained that, in parallel to IKKβ suppression, bFGF-induced suppression of NFκB activity was partly attributed to the suppression of transcriptional activity via S-nitrosylation of the p65 DNA binding domain. Taken together, these findings suggested that bFGF counteracted inflammation was partially attributed to the S-nitrosylation of IKKβ^{C179} and p65^{C38}.

3.4. bFGF-mediated S-nitrosylation of IKKβ^{C179} and p65^{C38} contributed to in vitro and in vivo angiogenic function under HG + PA conditions

We next investigated the potential link between S-nitrosylation, NFκB activity, and angiogenic functions of endothelial cells *in vitro* and

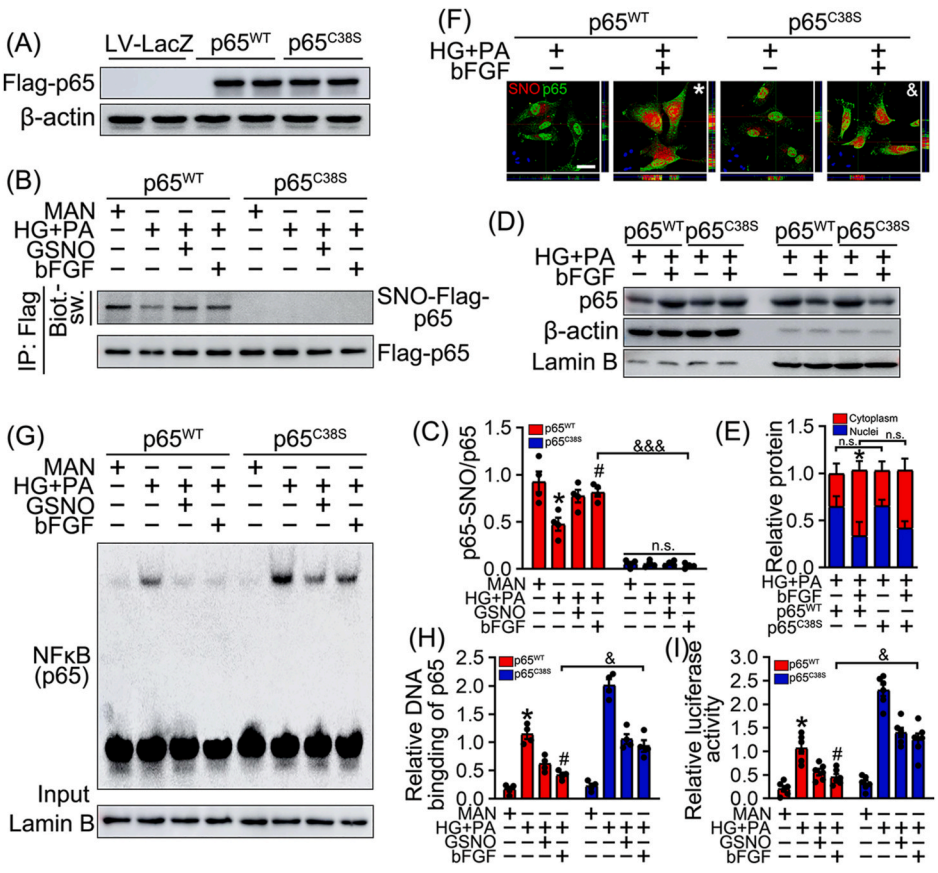

Fig. 4. bFGF mediated SNO-p65 contributes to the suppression of chronic inflammation. HUVECs were infected with a lentiviral vector encoding *LacZ* (control), wild-type p65 (*LV-p65^{WT}*), or mutant p65, in which Cys-38 was replaced with the non-nitrosylatable residue serine (*LV-p65^{C38S}*). After transfection, overexpression cells were established and selected with G418 and cultured either in MAN or HG + PA medium in the presence or absence of bFGF and GSNO for 72 h. (A) Representative immunoblotting images of Flag confirmed that the cells were transfected with entivirus successfully. (B) The mutation of p65^{C38S} abrogated bFGF mediated SNO-p65^{C38}, p65 protein loading was detected by anti-Flag antibody. (C) Quantification of S-nitrosylated protein levels (percentage of S-nitrosylated protein to total) in HUVECs, values displayed are means ± SEM of 4 independent experiments. One-way ANOVA with the Student-Newman-Keuls test was used. n. s. = not significant, *p < 0.05 vs. *LV-p65^{WT}*-transfected HUVECs cultured in MAN; #p < 0.05 vs. *LV-p65^{WT}*-transfected HUVECs cultured in HG + PA; &&& p < 0.001 vs. *LV-p65^{WT}*-transfected HUVECs cultured in bFGF. (D) Nuclear and cytosolic extracts made from HUVECs were isolated, and transfection of p65WT and non-nitrosylatable p65^{C38S} mutant exposure to HG + PA or bFGF respectively have none impact on the nuclear translocation of p65. (E) Quantification of p65 localization, values displayed are means ± SEM of 4 independent experiments, one-way ANOVA with the Student-Newman-Keuls test was used * p < 0.05 vs. *LV-p65^{WT}*-transfected HUVECs cultured in HG + PA, n. s. = not significant. (F) Fixed cells were subjected to a biotin-switch assay. S-nitrosylation was visualized using Alexa-568-conjugated avidin (red) and p65 nuclear translocation was determined by immunofluorescent staining (green) in HUVECs, the merged puncta (yellow) is the p65 closed proximity with S-nitrosated protein or SNO-p65 itself, nucleus was blue, Scale bars = 200 μm. One-way ANOVA with Bonferroni's correction was used, values displayed are means ± SEM of 3 independent experiments. *p < 0.05 vs. *LV-p65^{WT}* transfected HUVECs cultured in HG + PA; & p < 0.05 vs. *LV-p65^{WT}*-transfected HUVECs treatment with bFGF. (G) Transfection of non-nitrosylatable p65^{C38S} mutant increases the DNA binding ability of p65. EMSA assays were performed as described in "Materials and Methods". (H) The quantitative analysis of each immunoblots, values displayed are means ± SEM of 4 independent experiments. One-way ANOVA with the Student-Newman-Keuls test was used. *p < 0.05 vs. *LV-p65^{WT}*-transfected HUVECs cultured in MAN; #p < 0.05 vs. *LV-p65^{WT}*-transfected HUVECs cultured in HG + PA; &&& p < 0.001 vs. *LV-p65^{WT}*-transfected HUVECs cultured in bFGF. (I) Equal amounts of cell lysates were tested for luciferase activity as described in "Materials and Methods", values displayed are means ± SEM of 6 independent experiments. One-way ANOVA with the Student-Newman-Keuls test was used. *p < 0.05 vs. *LV-p65^{WT}*-transfected HUVECs cultured in MAN; #p < 0.05 vs. *LV-p65^{WT}*-transfected HUVECs cultured in HG + PA; &&& p < 0.001 vs. *LV-p65^{WT}*-transfected HUVECs cultured in bFGF. (For interpretation of the references to colour in this figure legend, the reader is referred to the Web version of this article.)

in vivo. Given the regulation effect of SNO-IKKβ^{C179} and SNO-p65^{C38} on NFκB transcriptional activity, loss of S-nitrosylation at these sites could trigger chronic inflammation under HG + PA conditions in HUVECs. We thus sought to explore whether SNO-IKKβ^{C179} or SNO-p65^{C38} affected the angiogenic functions of endothelial cells. *IKKβ^{WT}* + *p65^{WT}* and *IKKβ^{C179S}* + *p65^{C38S}* expression were stably established in cultured HUVECs. Expression of NFκB target genes were significantly increased in *IKKβ^{C179S}* + *p65^{C38S}* mutant-overexpressing HUVECs compared with wild-type-expressing HUVECs, consistent with the notion that loss of S-nitrosylation could trigger proinflammatory cytokines such as *IL-1β*, *IL-6*, *IL-8*, and *TNFα* (Supplementary Fig. 5A). Meanwhile, HG + PA impaired tube formation activity in *IKKβ^{WT}* + *p65^{WT}* overexpressed HUVECs were alleviated by bFGF, but largely abrogated in *IKKβ^{C179S}* + *p65^{C38S}*-overexpressed HUVECs (Fig. 5A and B). Besides, the similar results were also observed by cell migration assay (Supplementary Fig. 5B; Fig. 5C).

To further assess the endothelial protective function of bFGF-mediated IKKβ^{C179} and p65^{C38} S-nitrosylation, *KKβ^{WT}* + *p65^{WT}* or *IKKβ^{C179S}* + *p65^{C38S}* mutant overexpression were induced by lentiviral infection of aortic rings from *db/m* or *db/db* mice. During the experiment, the blood glucose was measured by glucose analyzer (Supplementary Table S1). Then, aortic rings were cultured in MAN or HG + PA media in the presence or absence of bFGF. A well-structured microvessel network with clearly defined tubules and regular branching was present in both *IKKβ^{WT}* + *p65^{WT}* and *IKKβ^{C179S}* + *p65^{C38S}* mutant-overexpressing aortic rings from *db/m* mice cultured in MAN medium (Fig. 5D and E). However, *IKKβ^{C179S}* + *p65^{C38S}* mutant overexpression significantly impaired sprouting function in rings exposed to HG + PA as compared with rings maintained in MAN, meanwhile, overexpression of mutant proteins abrogated the protective effect of bFGF in this context (Fig. 5D and E).

To further assess the roles of SNO-IKKβ^{C179} and SNO-p65^{C38} in bFGF-mediated endothelial protection, we utilized an *in vivo* skin wound healing model in T2DM *db/db* mice, in which chronic inflammation suppresses endothelial function and subsequent wound healing [45]. Adenoviruses expressing *Ikkβ^{WT}* + *p65^{WT}* or *Ikkβ^{C179S}* + *p65^{C38S}* mutants with the EC-specific vascular endothelial cadherin promoter (Ad-*Cdh5-Ikkβ^{WT}* + Ad-*Cdh5-p65^{WT}* or Ad-*Cdh5-Ikkβ^{C179S}* + Ad-*Cdh5-p65^{C38S}*) were delivered to wounded tissue in *db/m* and *db/db* mice through subcutaneous injection. Meanwhile, the blood glucose levels were

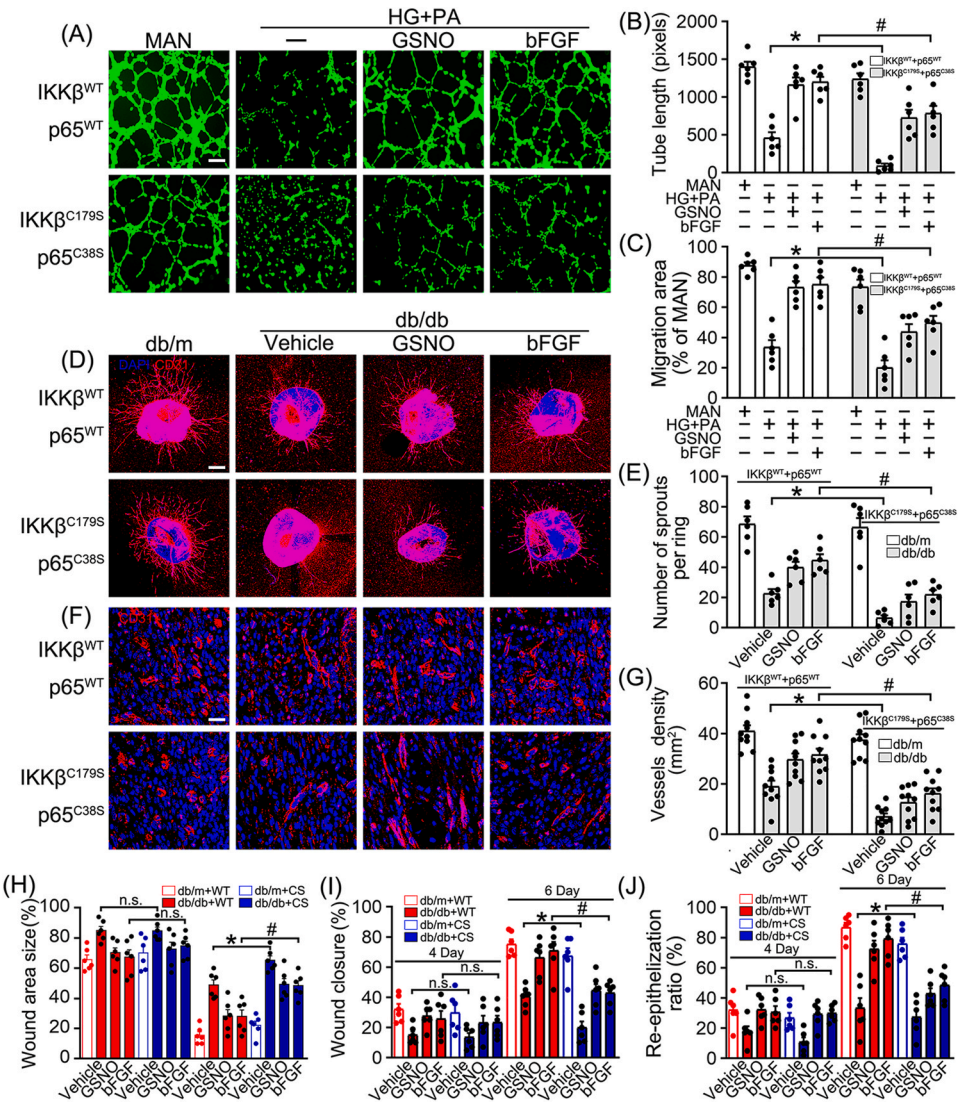

Fig. 5. Decomposition of S-nitrosylation contributes to cell death both in vitro and in vivo. (A–C) HUVECs were infected with a lentiviral vector encoding wild-type (*LV-IKKβ^{WT}; LV-p65^{WT}*), or a mutant was replaced with the non-nitrosylatable residue serine (*LV-IKKβ^{C179S}; LV-p65^{C38S}*). After transfection, overexpression cells were established and selected with G418 and puromycin respectively. (A) Capillary-like tube formation was assessed by matrigel angiogenesis assay in HUVECs. Scale bars = 75 μm. Overexpression of non-nitrosylatable p65^{C38S}-IKKβ^{C179S} reduce tube formation by ~50% in bFGF rescued cells (B) Quantification of the tube length in (A), images of tube morphology were taken in 6 random microscopic fields per sample and values displayed are means ± SEM of 6 independent experiments. Sample means were statistically significant as determined by a One-way ANOVA with the Student-Newman-Keuls, *p < 0.05; #p < 0.05. (C) Cell migration distances were measured based on the data (Supplementary Fig. 5b), with each data point representing the mean of multiple measures within a single well in a representative experiment, values displayed are means ± SEM of 6 independent experiments. One-way ANOVA with the Student-Newman-Keuls test was used. *p < 0.05; #p < 0.05. (D) Cultured aortic rings from db/m or db/db mice were overexpressed LV-p65^{WT} + IKKβ^{WT} or its LV-p65^{C38S} + IKKβ^{C179S} mutant respectively, then cultured in different mediums containing MAN and HG + PA in the presence and absence of bFGF. Scale bars = 350 μm. (E) Quantification of the number of sprouts in (D), values displayed are means ± SEM of 6 independent experiments. One-way ANOVA with the Student-Newman-Keuls test was used. *p < 0.05; #p < 0.05. (F–J) db/m and db/db mice were wounded on the back skin, and wound regions were intradermally injected with p65^{WT} (*Ad-Cdh5-p65^{WT}*) and IKKβ^{WT} (*Ad-Cdh5-IKKβ^{WT}*); p65^{C38S} (*Ad-Cdh5-p65^{C38S}*) and IKKβ^{C179S} (*Ad-Cdh5-IKKβ^{C179S}*). (F) CD31^{+} capillary density was imaged with a confocal laser scanning microscope at 4th day. Scale bars = 20 μm. (G) Quantification of the number of capillary density, n = 6/group, and images were taken in 10 random microscopy fields per sample, values displayed are means ± SEM. One-way ANOVA with the Student-Newman-Keuls test was used. *p < 0.05; #p < 0.05. (H) The wound area size (%) was measured for 6 days (Supplementary Fig. 5c), n = 6/group, values displayed are means ± SEM. One-way ANOVA with the Student-Newman-Keuls test was used. *p < 0.05; #p < 0.05. (I) The wound closing rate was measured for 6 days (Supplementary Fig. 5e) and quantified; n = 6/group, values displayed are means ± SEM. One-way ANOVA with the Student-Newman-Keuls test was used. *p < 0.05; #p < 0.05. (J) Measurement of reepithelization ratio (leading edge ratio) in wound area (Supplementary Fig. 5D and E), n = 6/group, and images were taken in 6 paraffin-embedded tissue sections per sample, values displayed are means ± SEM. One-way ANOVA with the Student-Newman-Keuls test was used. *p < 0.05; #p < 0.05.

determined. (Supplementary Table S2). We found that CD31^{+} capillary density was decreased in the regenerative skin tissue of *db/db* mice subcutaneously injected with Ad-*Cdh5-Ikkβ^{C179S}* + *p65^{C38S}* compared with that of *db/db* mice injected with Ad-*Cdh5-Ikkβ^{WT}* + *p65^{WT}*. Consistent with *in vitro* findings, bFGF treatment did not ameliorate CD31^{+} capillary density in *Ikkβ^{C179S}* + *p65^{C38S}*-overexpressing *db/db* mice compared with *Ikkβ^{WT}* + *p65^{WT}*-overexpressing *db/db* mice (Fig. 5F and G). In parallel, overexpression of *Ikkβ^{C179S}* + *p65^{C38S}* in endothelial cells delayed closure of the wound opening and abrogated the endothelial protective effect of bFGF in *db/db* mice (Supplementary Fig. 5C; Fig. 5H).

Although the gross wound size became comparable between *Cdh5-Ikkβ^{WT}* + *p65^{WT}* and *Cdh5-Ikkβ^{C179S}* + *p65^{C38S}*-overexpressing *db/db* mice on day 4 after wounding (Supplementary Fig. 5C; Fig. 5H), re-epithelialization was significantly decreased in *Ikkβ^{C179S}* + *p65^{C38S}*-overexpressing *db/db* mice relative to *Ikkβ^{WT}* + *p65^{WT}*-overexpressing *db/db* mice on day 6 (Supplementary Fig. 5D and E; Fig. 5J). Importantly, bFGF treatment unable to improve wound re-epithelialization in *Ikkβ^{C179S}* + *p65^{C38S}*-overexpressing *db/db* mice (Supplementary Fig. 5E; Fig. 5J). Additionally, histology analysis of wounds on day 6 after wounding revealed delayed wound closure and compromised re-epithelization in wounds from *db/db* mice overexpressing *Ikkβ^{C179S}* + *p65^{C38S}* compared with those from the *Ikkβ^{WT}* + *p65^{WT}*-overexpressing mice, which was particularly evident in the bFGF-treated group (Supplementary Fig. 5E; Fig. 5I and J). Taken together, these findings indicated that bFGF-mediated SNO-IKKβ^{C179} and SNO-p65^{C38} suppressed

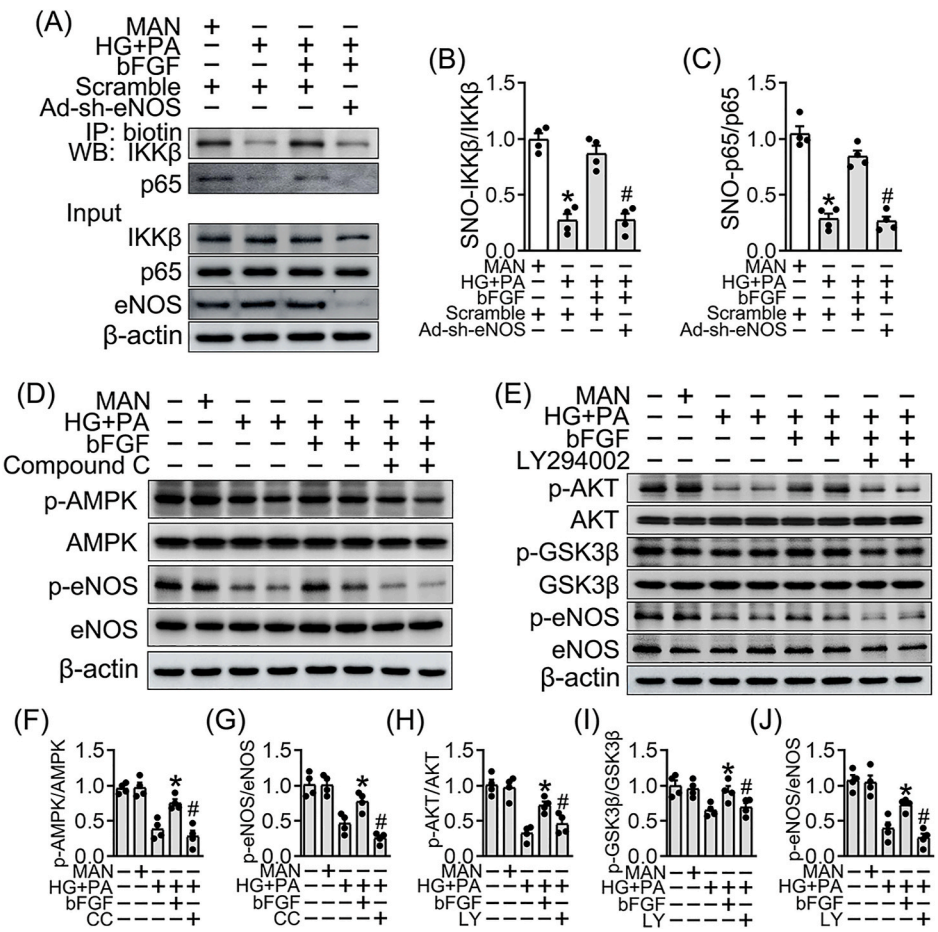

Fig. 6. bFGF induces eNOS-dependently S-nitrosylation of IKKβ and p65 through the Akt and Ampk pathway. (A) HUVECs were transfected with adenoviruses harboring human *sh-eNOS* (*Ad-sh-eNOS*) and a scrambled sequence (*Ad-scramble*) respectively. After transfection, HUVECs were cultured either in MAN or HG + PA medium in the presence or absence of bFGF for 72 h. Whole-cell lysates were subjected to the biotin switch assay as described in "Materials and Methods". In the absence of eNOS abolished bFGF induced S-nitrosylation of IKKβ and p65 in HUVECs. (B–C) Quantification of S-nitrosylated protein levels (percentage of S-nitrosylated protein to total) in HUVECs, values displayed are means ± SEM of 4 independent experiments. Two-tailed Student's *t*-test was used, *p < 0.05 vs. MAN; #p < 0.05 vs. HG + PA coincubated with bFGF. (D–E) HUVECs were pretreated with or without LY294002 (20 μM), compound C (10 μM) for 2 h and then exposed to MAN and HG + PA for 72 h in the presence or absence of bFGF. (F–J) Quantitative analysis of phosphorylation of Akt, GSK3β, AMPK and eNOS protein, values displayed are means ± SEM of 4 independent experiments. Two-tailed Student's *t*-test was used, *p < 0.05 vs. HG + PA; #p < 0.05 vs. HG + PA coincubated with bFGF.

NFκB activity and dramatically alleviated T2DM-associated endothelial dysfunction.

3.5. bFGF induced eNOS-dependent IKKβ and p65 S-nitrosylation through the Akt/AMPK axis

Our earlier finding demonstrated that HG + PA-induced iNOS regulated S-nitrosylation during late-stage HG + PA exposure, while decreased S-nitrosylation during early-stage HG + PA exposure was iNOS-independent (Fig. 1, Supplementary Fig. 1). Therefore, to investigate the contribution of eNOS-derived NO to bFGF-mediated IKKβ and p65 S-nitrosylation at early-stage of HG + PA exposure, *eNOS* gene expression was knocked down with an adenovirus harboring *eNOS-shRNA* in HUVECs. *eNOS* knockdown abolished bFGF-induced IKKβ and p65 S-nitrosylation in HUVECs (Fig. 6A–C). Furthermore, to determine whether the effect of bFGF was eNOS-mediated, HUVECs were treated with the classical eNOS upstream pathway antagonist LY294002 (LY) or AMPK inhibitor Compound C (CC), respectively. Consistently, LY and CC decreased Akt/GSK3β and AMPK phosphorylation, respectively. Meanwhile, both treatments decreased eNOS activity in HUVECs following HG + PA treatment (Fig. 6D–J). Moreover, the effects of bFGF on eNOS activity were significantly abolished by both LY and CC treatment, suggesting that bFGF enhanced eNOS activity was dependent on these pathways (Fig. 6D–J). Together, these results suggested that bFGF-mediated S-nitrosylation of IKKβ and p65 could be due in part to eNOS up-regulation and activation through the Akt and AMPK pathways.

3.6. bFGF-mediated IKKβ and p65 S-nitrosylation suppressed inflammation through a txnip-dependent mechanism

The mechanism underlying suppression of inflammation via bFGF-mediated S-nitrosylation was further explored. In fact, S-nitrosylation has emerged as a dominant regulatory mechanism of GSNOR and Trx-associated signal transduction [7,46]. Therefore, we determined whether alteration of GSNOR was involved in the S-nitrosylation of IKKβ and p65, and subsequent suppression of inflammation and increased vasculogenesis. We found that bFGF treatment did not alter the expression of GSNOR in HUVECs exposed to HG + PA (Fig. 7A and B), and these findings were corroborated by whole-cell quantitative RT-PCR (qRT-PCR) analysis (Fig. 7I). In contrast, although the GSNOR activity was not significantly affected in early-stage of HG + PA exposure, it experienced a slowly decline activity in a time-dependent manner after day 3 (Supplementary Fig. 6A; Fig. 7C), indicating that bFGF-mediated IKKβ and p65 S-nitrosylation was independent of GSNOR.

It is noteworthy that Trx modulates protein S-nitrosylation homeostasis, and acting as a double edge sword for the regulation of the cell fate. Forrester et al. reported that Trx-mediated protein denitrosylation is augmented by endogenously derived NO via repression of Txnip, which in turn protects against iNOS-mediated cell death [8]. On the contrary, it has been recently reported that Trx is essential for maintaining S-nitrosylation in endothelial cells [9], and can transfers $^{+}$NO to caspase-3, which leads to inhibition of apoptosis. To address this discrepancy, we determined whether Trx was involved in bFGF-mediated IKKβ and p65 S-nitrosylation in HUVECs. Similarly, we found that bFGF treatment did not affect Trx protein and mRNA levels in HUVECs exposed to HG + PA (Fig. 7D–F and 7I). The activity of Trx also decreased in a time-dependent manner during early-stage HG + PA

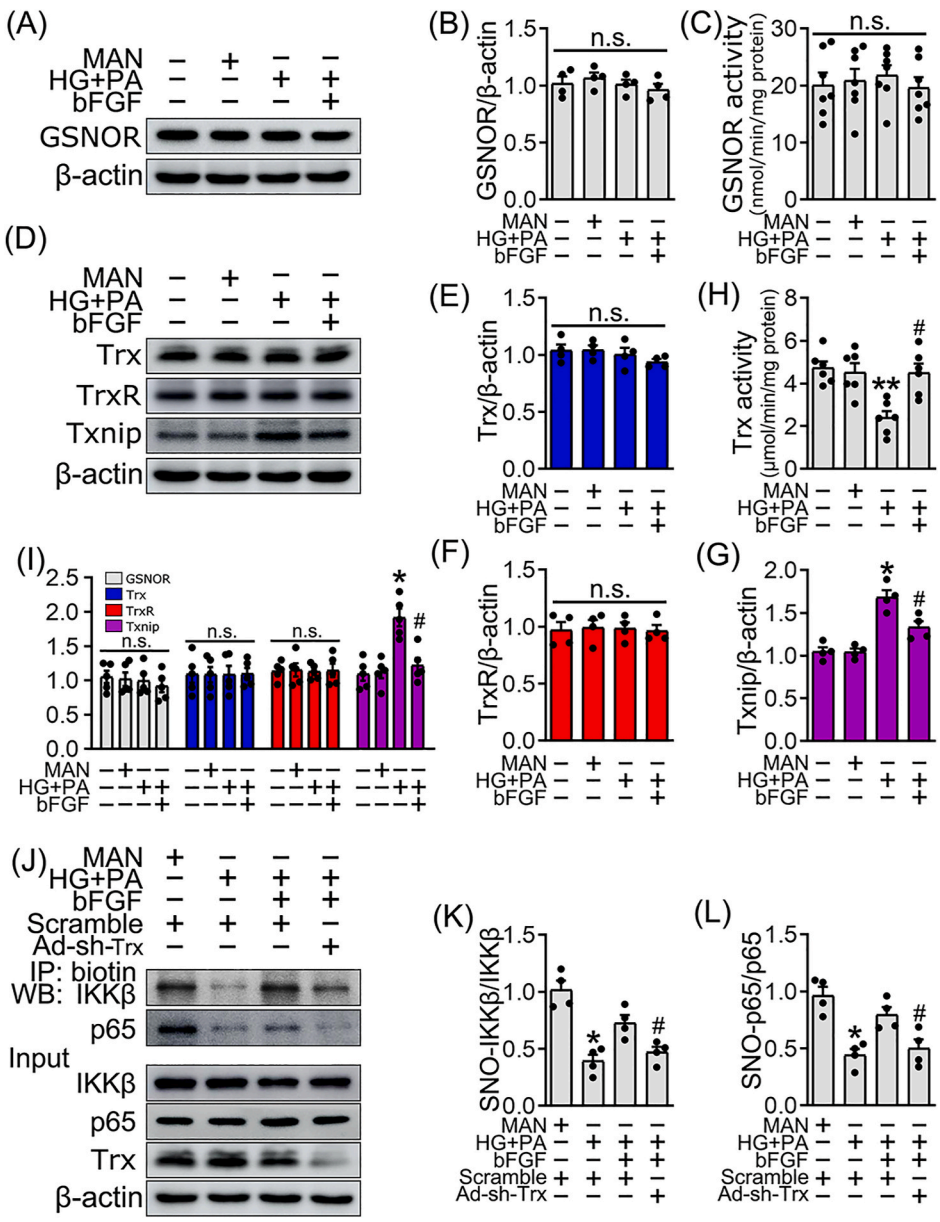

Fig. 7. bFGF-mediated S-nitrosylation of IKKβ and p65 through the Trx rather than GSNOR. (A–I) HUVECs were exposed to NG and HG + PA in the presence or absence of bFGF for 72 h. (A) Anti-GSNOR immunoblot analysis from whole-cell lysates confirms that bFGF treatment could not impact the expression of GSNOR proteins. (B) The quantitative analysis of GSNOR immunoblots, values displayed are means ± SEM of 4 independent experiments. Two-tailed Student's *t*-test was used, n. s. = not significant. (C) The mean GSNOR enzymatic activity in the HUVECs was no significant change at 3rd day; values displayed are means ± SEM of 6 independent experiments. Wilcoxon rank-sum test was used, n. s. = not significant. (D) Anti-Trx, TrxR and Txnip immunoblot analysis from whole-cell lysates confirms that bFGF treatment also could not impact the expression of Trx and TrxR proteins but bFGF treatment decrease the protein level of the Txnip. (E–G) The quantitative analysis of Trx, TrxR and Txnip immunoblots, values displayed are means ± SEM of 4 independent experiments. Two-tailed Student's *t*-test was used, n. s. = not significant, *p < 0.05 vs. NG or MAN; #p < 0.05 vs. HG + PA. (H) The mean Trx enzymatic activity in the HUVECs. Values displayed are means ± SEM of 6 independent experiments. Wilcoxon rank-sum test was used, **p < 0.01 vs. NG or MAN; #p < 0.05 vs. HG + PA. (I) mRNA expression of GSNOR, Trx and TrxR genes. Values displayed are means ± SEM of 5 independent experiments. Two-tailed Student's *t*-test was used, n. s. = not significant, *p < 0.05 vs. NG or MAN; #p < 0.05 vs. HG + PA. (J) HUVECs were transfected with adenoviruses harboring human *sh-Trx* (*Ad-sh-Trx*) and a scrambled sequence (*Ad-scramble*) respectively. After transfection, HUVECs were cultured either in MAN or HG + PA medium in the presence or absence of bFGF for 72 h. Whole-cell lysates were subjected to the biotin switch assay as described in "Materials and Methods". (K–L) Quantification of S-nitrosylated protein levels (percentage of S-nitrosylated protein to total) in HUVECs, values displayed are means ± SEM of 4 independent experiments. Two-tailed Student's *t*-test was used, *p < 0.05 vs. MAN; #p < 0.05 vs. HG + PA coincubated with bFGF.

exposure, and subsequently recovered and increased by day 5 (Supplementary Fig. 6B). Interestingly, the declined activity of Trx at day 3 was significantly ameliorated by bFGF treatment (Fig. 7H). To investigate the contribution of Trx regulation to bFGF-mediated IKKβ and p65 S-nitrosylation, *Trx* gene expression was knocked down with an adenovirus harboring *Trx-shRNA* in HUVECs. Trx ablation partially abolished bFGF-regulated IKKβ and p65 S-nitrosylation in HUVECs (Fig. 7J–L). Additionally, protein levels of other major redox enzyme protein systems (Supplementary Fig. 6C–E) and major NOS isoforms (Supplementary Fig. 6C, F–G) were unaffected by silencing of Trx in HUVECs. Nevertheless, Trx deficiency abolished itself activity (Supplementary Fig. 6H), and partially weakening bFGF promotion of NO availability, demonstrating that the promotion effect of Trx on NO availability was mainly attribute to ROS neutralization and cellular redox homeostasis maintenance during the window of the initial of inflammation, which in turn contributed to bFGF-mediated IKKβ and p65 S-nitrosylation subsequently.

On the other hand, to eliminate the potential function exerts by the interaction of Trx with p65 and IKKβ, which possible to regulate the S-nitrosylation state of p65 and IKKβ contributed by bFGF treatment, immunoprecipitation was performed. We found that the interaction between Trx and P65 were slightly decreased by HG + PA treatment at day 3, even in the presence of bFGF. While, totally no interaction was detected between Trx and IKKβ (Supplementary Fig. 7A). Taken together, these data indicated that Trx was essential for maintaining the homeostasis of S-nitrosylated molecules in endothelial cells, and bFGF-mediated SNO-IKKβ^{C179} and SNO-p65^{C38} through a mechanism attribute to the alteration of Trx activity rather than GSNOR.

Meanwhile, thioredoxin-interacting protein (Txnip) has originally been described as a negative Trx regulator that represses Trx activity through protein–protein interaction [47]. Therefore, we investigated whether Txnip was involved in bFGF-mediated IKKβ and p65 S-nitrosylation. bFGF significantly decreased Txnip protein level in HUVECs treated with HG + PA (Fig. 7D, G). Thereafter, we evaluated whether bFGF-mediated Txnip alteration contributed to the interaction between Txnip and Trx. Immunoprecipitation analysis revealed that bFGF decreased the association of Txnip with Trx (Fig. 8A and B). However, forced overexpression of *Txnip* abolished bFGF-mediated dissociation of Txnip and Trx (Fig. 8A and B). In addition, *Txnip* overexpression weakened Trx activity (Fig. 8C) and bioactivity of NO, and thus partly

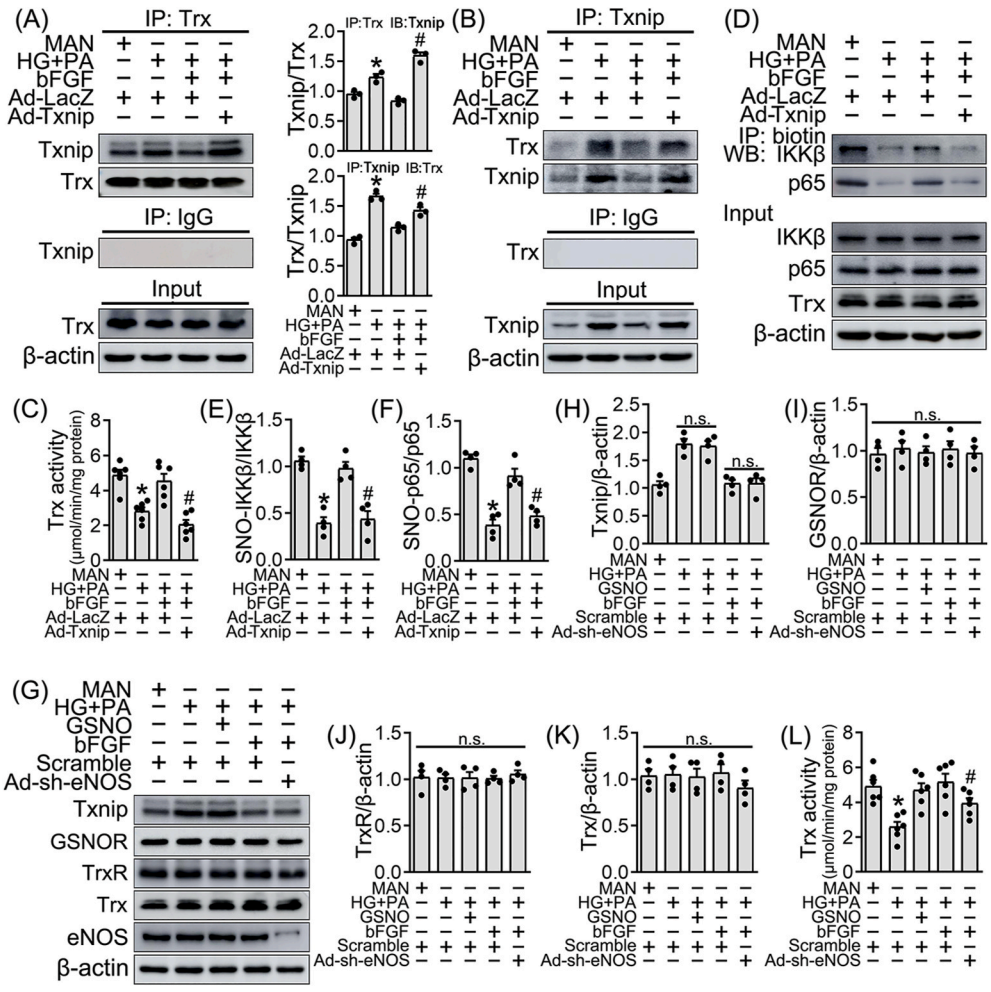

Fig. 8. bFGF mediated S-nitrosylation of IKKβ and p65 regulates anti-inflammation through a mechanism involving Txnip. (A–F) HUVECs were transfected with adenoviruses harboring human *Txnip* (*Ad-Txnip*) and *Ad-LacZ* (served as a control) respectively. After transfection, HUVECs were cultured either in MAN or HG + PA medium in the presence or absence of bFGF for 72 h. (A) The cell lysates were subjected to immunoprecipitation with Trx antibody, followed by immunoblotting with the indicated antibodies. Cell lysates were also subjected to immunoprecipitation with IgG as negative control. Quantification of interaction between Trx and Txnip in HUVECs (IP: Trx, IB: Txnip), values displayed are means ± SEM of 3 independent experiments. Two-tailed Student's *t*-test was used, *p < 0.05 vs. MAN; #p < 0.05 vs. HG + PA coincubated with bFGF (right panel). (B) The cell lysates were subjected to immunoprecipitation with Txnip antibody, followed by immunoblotting with the indicated antibodies. Cell lysates were also subjected to immunoprecipitation with IgG as negative control. Quantification of interaction between Txnip and Trx in HUVECs (IP: Txnip, IB: Trx), values displayed are means ± SEM of 3 independent experiments. Two-tailed Student's *t*-test was used, *p < 0.05 vs. MAN; #p < 0.05 vs. HG + PA coincubated with bFGF (left panel). (C) Overexpression of Txnip weaken the activity of Trx, values displayed are means ± SEM of 6 independent experiments. Wilcoxon rank-sum test was used, *p < 0.05 vs. MAN; #p < 0.05 vs. HG + PA coincubated with bFGF. (D) Whole-cell lysates were subjected to the biotin switch assay as described in "Materials and Methods". (E–F) Quantification of S-nitrosylated protein levels (percentage of S-nitrosylated protein to total) in HUVECs, values displayed are means ± SEM of 4 independent experiments. Two-tailed Student's *t*-test was used, *p < 0.05 vs. MAN; #p < 0.05 vs. HG + PA coincubated with bFGF. (G) HUVECs were transfected with adenoviruses harboring human *sh-eNOS* (*Ad-sh-eNOS*) and a scrambled sequence (*Ad-scramble*) respectively. After transfection, HUVECs were cultured either in MAN or HG + PA medium in the presence or absence of bFGF or GSNO for 72 h. Related protein immunoblot analysis from whole-cell lysates. (H–K) The quantitative analysis of related protein immunoblots, values displayed are means ± SEM of 4 independent experiments. Two-tailed Student's *t*-test was used, n. s. = not significant. (L) Deficiency of eNOS partly abolished the bFGF promoted Trx activity. Values displayed are means ± SEM of 6 independent experiments. Wilcoxon rank-sum test was used, *p < 0.05 vs. MAN; #p < 0.05 vs. HG + PA coincubated with bFGF.

abolished bFGF-mediated IKKβ and p65 S-nitrosylation (Fig. 8D–F). Overall, these results suggested that bFGF-mediated IKKβ, and p65 S-nitrosylation was attributed at least in part through the suppression of Txnip, which promoted disassociation of Txnip and Trx, subsequently maintaining the content of S-nitrosylated molecules in endothelial cells.

Although endogenously derived NO repressed Txnip expression [8], and bFGF promoted eNOS activation via the Akt/AMPK axis (Fig. 6D–J), bFGF also decreased expression of Txnip in *eNOS* knockdown HUVECs (Fig. 8G and H). Further results showed that GSNO stimulation did not affect hyperglycemia enhanced promoter activity of Txnip (Fig. 8G and H), demonstrated that bFGF affected the expression of Txnip in a NO-independent manner. Besides, other major redox enzyme protein systems (Fig. 8G, I–K) were also not affected by bFGF treatment with silencing of eNOS in HUVECs, but partly abolished bFGF-promoted Trx activity (Fig. 8L). In addition, we found that HG + PA-mediated dissociation of Trx and eNOS were reversed by bFGF (Supplementary Fig. 7B), and bFGF mediated S-nitrosylation of Trx was eNOS dependent in HUVECs (Supplementary Fig. 7C and D). Taken together, these findings suggested that bFGF-mediated IKKβ and p65 S-nitrosylation were mainly attributed to synergy between eNOS and Trx activity.

4. Discussion

S-nitrosylation, a redox-based post-translational modification of proteins by NO, is recognized to regulate the activities of an increasing number of target proteins, including metabolic, structural, cytoskeletal, and signaling proteins [48]. Recent studies provided strong evidence that S-nitrosylation negatively regulates inflammation [49]. In the present study, we demonstrate that bFGF exerts its endothelial protective action against hyperglycemia (HG) and hyperlipidemia (PA) impairment, at least in part, through delaying and inhibiting diabetes triggered excessive chronic inflammation at early stage. And this process is partly mediated via promoting S-nitrosylation of IKKβ^{C179} and p65^{C38} instead of the routine pathway.

Protein S-nitrosylation affects a broad spectrum of human diseases, including cardiovascular, pulmonary, musculoskeletal, and neurological

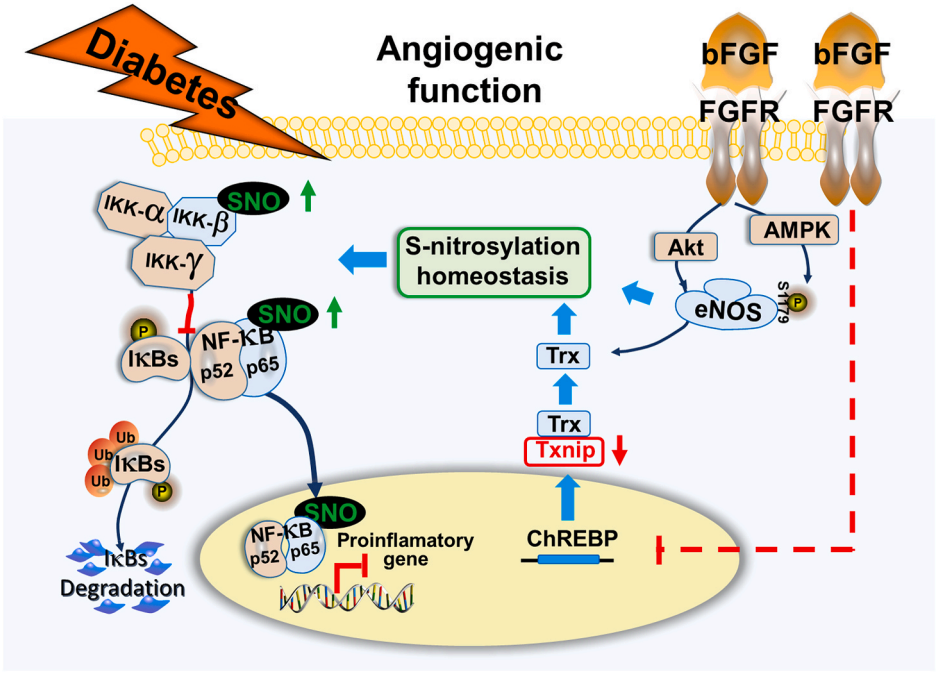

Fig. 9. Schematic illustration of the protective effects of bFGF on HUVECs under HG + PA conditions. Diabetes-induced endothelial impairment can be attributed mainly to the dysfunction of S-nitrosylation homeostasis (S-nitrosylation of IKKβ^{C179} and p65^{C38}) and resultant upregulation of chronic inflammation. Mechanistically, the upregulation of S-nitrosylated IKKβ^{C179} and p65^{C38} by bFGF were attributed to the synergy between eNOS and Trx activity. In addition, the bFGF-mediated disassociation between Txnip and Trx in a NO-independent manner, also benefited the cellular redox homeostasis and maintaining the content of S-nitrosylated IKKβ^{C179} and p65^{C38} in endothelial cells. This finding could yield new therapeutic insights into the prevention and treatment of diabetes-associated vascular disease.

disorders, as well as cancer [50]. However, the role of S-nitrosylation in diabetic vascular disease has not been fully evaluated. Recent research revealed that obesity-associated chronic inflammation is a major factor in metabolic tissues such as liver and skeletal muscle, which contributes to insulin resistance via a common pathway of aberrant protein S-nitrosylation [51]. Meanwhile, high glucose alone induced superoxides could induce the breakdown of protein S-nitrosolation in endothelial cells [16]. Although the role of iNOS-induced aberrant protein S-nitrosylation in metabolic tissues occurs during late-stage T2DM [52], less is known about the impact of S-nitrosylation on vascular endothelial dysfunction prior to T2DM-triggered chronic inflammation. Additionally, in the present study, HG and PA were used as the *in vitro* stimuli to mimic the diabetic condition, which makes more sense compare with the only single condition (HG or PA alone), even HG [16] or aliphatic acid (exc. oxLDL) [14] could impact on protein S-nitrosylation separately.

To elucidate the detailed mechanisms of development or progression of diabetes-triggered chronic inflammation, HUVECs were cultured with mild hyperglycemia and hyperlipidemia (HG + PA) over a time course. Not surprisingly, HG + PA exposure biphasically affected protein S-nitrosylation, with early impairment of S-nitrosylation (days 1–3) and late-stage recovery of S-nitrosylation (days 4–5). Therefore, we focused on the time frame of aberrant protein *S*-nitrosylation alteration, which occurs prior to initiation of the inflammatory response in diabetes-triggered vascular endothelial dysfunction. Although levels of most *S*-nitrosylated proteins were decreased on day 3 of HG + PA treatment, S-nitrosylation of some proteins was either increased or unchanged, suggesting protein-specific regulation of S-nitrosylation in early T2DM. *S*-nitrosylation has been implicated in the regulation of numerous protein activities [5], the finding that HG + PA regulated protein *S*-nitrosylation (SNO-IKKβ and SNO-p65) in HG + PA-treated endothelial cells could provide new insights into the mechanisms underlying early diabetic vascular injury. Consequently, in this study, increased inflammation in the vascular endothelium of *db/db* mice as well as HG + PA-treated HUVECs were observed. In addition, bFGF restored *in vivo* endothelial function was decreased in *db/db* mice expressing mutant S-nitrosylation-resistant IKKβ and p65 at wound sites. Thus, a detrimental role for early-stage inflammation regulated in part by decreased IKKβ and p65 S-nitrosylation that alleviated by bFGF was proved.

NFκB is a master transcription factor that regulates multiple genes critically involved in the regulation of endothelial function and is central to the pathogenesis of various vascular disorders. Moreover, mounting evidence suggests that S-nitrosylation is a major NO-dependent post-translational mechanism that directly regulates protein function [53]. For example, aerosolized LPS induces iNOS expression in the respiratory epithelium concomitant with increased SNO-p65 levels and decreased airway NFκB activity. In contrast, genetic deletion of iNOS decreases SNO-p65, resulting in persistent NFκB activity and prolonged airway inflammation [54]. Meanwhile, 17-estradiol stimulates protein S-nitrosylation by increasing eNOS-generated NO in HUVECs [55]. Corresponding with this view, in the present study, we found that HG + PA decreased protein S-nitrosylation in HUVECs were alleviated by bFGF, and IKKβ and p65 were implicated as direct target for S-nitrosylation. We also reveal that bFGF-mediated endothelial protection through a mechanism involving SNO-IKKβ and SNO-p65 with a NO bioavailability dependent manner.

S-nitrosylation of target proteins is influenced by the formation of biologically relevant nitrosylating species and the rate of denitrosylation [48]. S-nitrosoglutathione reductase (GSNOR) is an NADH-dependent oxidoreductase that specifically breaks down GSNO, impairing protein S-nitrosylatoin [56]. However, in the present study, we demonstrated that the bFGF-mediated SNO-IKKβ and SNO-p65 suppressed inflammation through a GSNOR-independent mechanism. On the other hand, thioredoxin/thioredoxin reductases (Trx/TrxR), important for neutralizing ROS and maintaining redox balance, also exert vital function on protein S-nitrosylation homeostasis. Meanwhile, S-nitrosated Trx (SNO-Trx^{C69}, SNO-Trx^{C62}, SNO-Trx^{C32}, SNO-Trx^{C35}) is required for scavenging reactive oxygen species and for preserving the redox regulatory activity of Trx [57]. Furthermore, a recent report demonstrated that superoxide might induce decomposition of S-nitrosothiols in a dose- and time-dependent manner, and high glucose-mediated NFκB S-denitrosylation could be completely reversed by ROS inhibition [16]. Intricately but briefly, in the present study, we identified that bFGF-mediated disassociation between Txnip and Trx [47], benefited the cellular redox homeostasis and maintaining the content of S-nitrosylated IKKβ^{C179} and p65^{C38} in endothelial cells. In addition, we found that HG + PA abolished the effects of NO on Txnip promoter activity, even with GSNO stimulation, and bFGF down-regulated Txnip and decreased its association with Trx with an eNOS independent mode.

These results implied that bFGF affected Txnip expression and Trx inactivation via a NO-independent mechanism.

Collectively, in the present study, we reported for the first time that hyperglycemia and hyperlipidemia globally attenuated protein S-nitrosylation in HUVECs. The protective effects of bFGF on hyperglycemia- and hyperlipidemia-induced endothelial impairment could be partially attributed to its role in maintaining S-nitrosylation homeostasis and the resultant suppression of inflammation. Furthermore, bFGF suppressed hyperglycemia/hyperlipidemia-induced inflammation via SNO-IKKβ and SNO-p65 was eNOS-dependent, and involved a synergistic NO-independent repression of Txnip (Fig. 9). Although bFGF has not developed to be used in clinics since it has cell-stimulating effects (potential tumor formation), this finding could yield new therapeutic insights into the diabetic non-healing skin ulcers and treatment of diabetes-associated vascular disease with shortly and targeted treatment in future.

Funding

This work was supported by the National Natural Science Foundation of China under Grants [81770498, 81773346, 82070507 and 81800236], the Key Scientific Project of MOST, China [grant number 2017YFA0506000]; the Natural Science Foundation of Zhejiang Province [grant number LZ21H020002].

Author contributions

W.T.C., J.X., L.T.J., X.K.L., and K.K. designed the research and obtained material support and study supervision. G.C., N.A. and W.J.Y. performed the animal studies. G.C., N.A., Y.J.C., Z.C.H. and J.J.Z. performed the fluorescence experiments. G.C., S·H., W.J.G., E.Z.S., G.Z.T., Y.Z., L.X.F and C·Y.C. analyzed the data, wrote and edited the manuscript. All authors reviewed the manuscript.

Duality of interest

No potential conflicts of interest relevant to this article were reported.

Declaration of competing interest

The authors declare that they have no known competing financial interests or personal relationships that could have appeared to influence the work reported in this paper.

Acknowledgments

The authors thank the study volunteers for their participation.

Appendix A. Supplementary data

Supplementary data to this article can be found online at https://doi.org/10.1016/j.redox.2021.101904.

References

[1] K.E. Bornfeldt, I. Tabas, Insulin resistance, hyperglycemia, and atherosclerosis, Cell Metabol. 14 (2011) 575–585.
[2] S.M. Grundy, et al., Prevention Conference VI: diabetes and Cardiovascular Disease: executive summary: conference proceeding for healthcare professionals from a special writing group of the American Heart Association, Circulation 105 (2002) 2231–2239.
[3] D. Seth, A. Hausladen, Y.J. Wang, J.S. Stamler, Endogenous protein S-Nitrosylation in E. coli: regulation by OxyR, Science 336 (2012) 470–473.
[4] B.W. Yun, et al., S-nitrosylation of NADPH oxidase regulates cell death in plant immunity, Nature 478 (2011) 264–268.
[5] D.T. Hess, A. Matsumoto, S.O. Kim, H.E. Marshall, J.S. Stamler, Protein S-nitrosylation: purview and parameters, Nat. Rev. Mol. Cell Biol. 6 (2005) 150–166.
[6] D. Seth, et al., A multiplex enzymatic machinery for cellular protein S-nitrosylation, Mol. Cell. 69 (2018) 451–464.
[7] K. Kaliyaperumal, et al., S-Nitrosoglutathione-mediated STAT3 regulation in efficacy of radiotherapy and cisplatin therapy in head and neck squamous cell carcinoma, Redox Biol 6 (2015) 41–50.
[8] M.T. Forrester, et al., Thioredoxin-interacting protein (Txnip) is a feedback regulator of S-nitrosylation, J. Biol. Chem. 284 (2009) 36160–36166.
[9] J. Haendeler, et al., Redox regulatory and anti-apoptotic functions of thioredoxin depend on S-nitrosylation at cysteine 69, Nat. Cell Biol. 4 (2002) 743–749.
[10] S.M. Haldar, J. S. S-nitrosylation Stamler, Integrator of cardiovascular performance and oxygen delivery, J. Clin. Invest. 123 (2013) 101–110.
[11] E.T. Chouchani, et al., Cardioprotection by S-nitrosation of a cysteine switch on mitochondrial complex I, Nat. Med. 19 (2013) 753–759.
[12] L. Yang, et al., METABOLISM: S-Nitrosylation links obesity-associated inflammation to endoplasmic reticulum dysfunction, Science 349 (2015) 500–506.
[13] A. Martinez-Ruiz, S. Lamas, Detection and proteomic identification of S-nitrosylated proteins in endothelial cells, Arch. Biochem. Biophys. 423 (2004) 192–199.
[14] J. Hoffmann, J. Haendeler, A.M. Zeiher, S. Dimmeler, TNFalpha and oxLDL reduce protein S-nitrosylation in endothelial cells, J. Biol. Chem. 276 (2001) 41383–41387.
[15] J. Hoffmann, S. Dimmeler, J. Haendeler, Shear stress increases the amount of S-nitrosylated molecules in endothelial cells: important role for signal transduction, FEBS Lett. 551 (2003) 153–158.
[16] C. Wadham, A. Parker, L. Wang, P. Xia, High glucose attenuates protein S-nitrosylation in endothelial cells: role of oxidative stress, Diabetes 56 (2007) 2715–2721.
[17] E. Tanaka, K. Ase, T. Okuda, M. Okumura, K. Nogimori, Mechanism of acceleration of wound healing by basic fibroblast growth factor in genetically diabetic mice, Biol. Pharm. Bull. 19 (1996) 1141–1148.
[18] T. Nakamura, et al., Stimulation of endosteal bone formation by systemic injections of recombinant basic fibroblast growth factor in rats, Endocrinology 136 (1995) 1276–1284.
[19] J. Stark, et al., Basic fibroblast growth factor stimulates angiogenesis in the hindlimb of hyperglycemic rats, J. Surg. Res. 79 (1998) 8–12.
[20] M. Simons, et al., Pharmacological treatment of coronary artery disease with recombinant fibroblast growth factor-2: double-blind, randomized, controlled clinical trial, Circulation 105 (2002) 788–793.
[21] S.N. Nikolopoulos, P. Blaikie, T. Yoshioka, W. Guo, F.G. Giancotti, Integrin beta 4 signaling promotes tumor angiogenesis, Canc. Cell 6 (2004) 471–483.
[22] L. Vucicevic, et al., Compound C induces protective autophagy in cancer cells through AMPK inhibition-independent blockade of Akt/mTOR pathway, Autophagy 7 (2011) 40–50.
[23] J.W. Lee, et al., TLR4 (toll-like receptor 4) activation suppresses autophagy through inhibition of FOXO3 and impairs phagocytic capacity of microglia, Autophagy 15 (2019) 753–770.
[24] D. Kalra, et al., Nitric oxide provokes tumor necrosis factor-alpha expression in adult feline myocardium through a cGMP-dependent pathway, Circulation 102 (2000) 1302–1307.
[25] L. Tan, et al., Development of covalent inhibitors that can overcome resistance to first-generation FGFR kinase inhibitors, Proc. Natl. Acad. Sci. U. S. A. 111 (2014) 4869–4877.
[26] S.A. Gomes, et al., S-nitrosoglutathione reductase (GSNOR) enhances vasculogenesis by mesenchymal stem cells, Proc. Natl. Acad. Sci. U. S. A. 110 (2013) 2834–2839.
[27] G. Chen, et al., Baicalin alleviates hyperglycemia-induced endothelial impairment 1 via Nrf 2, J. Endocrinol. 240 (2018) 81–98.
[28] Y. Maejima, et al., Mst1 inhibits autophagy by promoting the interaction between Beclin 1 and Bcl-2, Nat. Med. 19 (2013) 1478–1488.
[29] J.A. Alva, et al., VE-Cadherin-Crerecombinase transgenic mouse: a tool for lineage analysis and gene deletion in endothelial cells, Dev. Dynam. 235 (2006) 759–767.
[30] H. Su, et al., Acute hyperglycaemia enhances oxidative stress and aggravates myocardial ischaemia/reperfusion injury: role of thioredoxin-interacting protein, J. Cell Mol. Med. 17 (2013) 181–191.
[31] J.F. Perz, G.L. Armstrong, L.A. Farrington, Y.J. Hutin, B.P. Bell, The contributions of hepatitis B virus and hepatitis C virus infections to cirrhosis and primary liver cancer worldwide, J. Hepatol. 45 (2006) 529–538.
[32] S.R. Jaffrey, S.H. Snyder, The biotin switch method for the detection of S-nitrosylated proteins, Sci. STKE 2001 (2001) pl1.
[33] N. Sen, et al., Hydrogen sulfide-linked sulfhydration of NF-kB mediates its antiapoptotic actions, Mol. Cell. 45 (2012) 13–24.
[34] M. Baker, et al., Use of the mouse aortic ring assay to study angiogenesis, Nat. Protoc. 7 (2011) 89–104.
[35] B. Tavora, et al., Endothelial FAK is required for tumour angiogenesis, EMBO Mol. Med. 8 (2016) 1229.
[36] A. Das, et al., Impairment of an endothelial NAD+-H2S signaling network is a reversible cause of vascular aging, Cell 176 (2019) 944–945.
[37] S. Jain, R. Gupta, R. Sen, Rho-dependent transcription termination in bacteria recycles RNA polymerases stalled at DNA lesions, Nat. Commun. 10 (2019) 1207.
[38] D. Li, et al., MicroRNA-132 enhances transition from inflammation to proliferation during wound healing, J. Clin. Invest. 125 (2015) 3008–3026.
[39] Safferling Kai, et al., Wound healing revised: a novel re-epithelialization mechanism revealed by in vitro and in silico models, J. Cell Biol. 203 (2013) 691–709.

[40] McBride Jeffrey, et al., Elevated circulation levels of an anti-angiogenic SERPIN in patients with diabetic microvascular complications impairs wound healing through suppression of wnt signaling, J. Invest. Dermatol. 134 (2014) 1725–1734.
[41] S. Thibeault, et al., S-nitrosylation of b-catenin by eNOS-derived NO promotes VEGF-induced endothelial cell permeability, Mol. Cell. 39 (2010) 468–476.
[42] V.F. Shih, R. Tsui, A. Caldwell, A.A. Hoffmann, Single NFκB system for both canonical and non-canonical signaling, Cell Res. 21 (2011) 86–102.
[43] H.E. Marshall, J.S. Stamler, Inhibition of NF-kappa B by S-nitrosylation, Biochemistry 40 (2001) 1688–1693.
[44] N.L. Reynaert, et al., Nitric oxide represses inhibitory B kinase through S-nitrosylation, Proc. Natl. Acad. Sci. U. S. A. 101 (2004) 8945–8950.
[45] M. Kulkarni, et al., Use of a fibrin-based system for enhancing angiogenesis and modulating inflammation in the se of a fibrin-based system for enhancing angiogenesis and se of a fibrin-based system for enhancing angiogenesis and, Biomaterials 35 (2014) 2001–2010.
[46] B.C. Smith, M.A. Marletta, Mechanisms of S-nitrosothiol formation and selectivity in nitric oxide signaling, Curr. Opin. Chem. Biol. 16 (2012) 498–506.
[47] S.T. Pang, et al., Thioredoxin-interacting protein: an oxidative stress-related gene is upregulated by glucose in human prostate carcinoma cells, J. Mol. Endocrinol. 42 (2009) 205–214.
[48] J.S. Stamler, S. Lamas, F.C. Fang, Nitrosylation the prototypic redox-based signaling mechanism, Cell 106 (2001) 675–683.
[49] H.E. Marshall, D.T. Hess, J.S. Stamler, S-nitrosylation, physiological regulation of NF-kappaB, Proc. Natl. Acad. Sci. U. S. A. 101 (2004) 8841–8842.
[50] M.W. Foster, D.T. Hess, J.S. Stamler, Protein S-nitrosylation in health and disease: a current perspective, Trends Mol. Med. 15 (2009) 391–404.
[51] Q. Qian, et al., T7: S-nitrosoglutathione reductase dysfunction contributes to obesity-associated hepatic insulin resistance via regulating autophagy, Diabetes 67 (2018) 193–207.
[52] M.A. Carvalho-Filho, et al., S-nitrosation of the insulin receptor, insulin receptor substrate 1, and protein kinase B/Akt: a novel mechanism of insulin resistance, Diabetes 54 (2005) 959–967.
[53] A. Martínez-Ruiz, S. Cadenas, S. Lamas, Nitric oxide signaling: classical, less classical, and nonclassical mechanisms, Free Radic. Biol. Med. 51 (2011) 17–29.
[54] Z.T. Kelleher, et al., NOS2 regulation of LPS-induced airway inflammation via S-nitrosylation of NF-{kappa}B p65, Am. J. Physiol. Lung Cell Mol. Physiol. 301 (2011) 327–333.
[55] S. Chakrabarti, O. Lekontseva, A. Peters, S.T. Davidge, 17 beta-Estradiol induces protein S-nitrosylation in the endothelium, Cardiovasc. Res. 85 (2010) 796–805.
[56] L. Liu, et al., A metabolic enzyme for S-nitrosothiol conserved from bacteria to humans, Nature 410 (2001) 490–494.
[57] D.A. Mitchell, et al., Thioredoxin is required for S-nitrosation of procaspase-3 and the inhibition of apoptosis in Jurkat cells, Proc. Natl. Acad. Sci. U.S.A. 104 (2007) 11609–11614.